On the distribution of spinal premotor interneurons

Remi Ronzano[*1], Sophie Skarlatou[*2], B. Anne Bannatyne[*3], Gardave S. Bhumbra[*4], Joshua D. Foster[4], Camille Lancelin[1], Amanda Pocratsky[1], Mustafa Görkem Özyurt[1], Calvin C. Smith[1], Andrew J. Todd[3], David J. Maxwell[3], Andrew J. Murray[5], Robert M. Brownstone[1§], Niccolò Zampieri[2§], Marco Beato[3§]

[1] Department of Neuromuscular Diseases, UCL Queen Square Institute of Neurology, University College London, London WC1N 3BG, UK

[2] Max Delbrück Center for Molecular Medicine (MDC), Robert-Rössle-Str. 10, 13092 Berlin, Germany

[3] Institute of Neuroscience and Psychology, College of Medical, Veterinary and Life Sciences, University of Glasgow, West Medical Building, Glasgow G12 8QQ, UK

[4] Department of Neuroscience Physiology and Pharmacology (NPP), Gower Street, University College London, WC1E 6BT, UK

[5] Sainsbury Wellcome Centre for Neural Circuits and Behaviour, University College London, London W1T 4JG, UK

*equal contribution

[§]co-senior authors

Corresponding authors:

Niccolò Zampieri, Max Delbrück Center for Molecular Medicine (MDC), Robert-Rössle-Str. 10, 13092 Berlin, Germany

niccolo.zampieri@mdc-berlin.de

Robert M. Brownstone, Department of Neuromuscular Diseases, UCL Queen Square Institute of Neurology, University College London, London WC1N 3BG, UK

r.brownstone@ucl.ac.uk

Marco Beato, Department of Neuroscience Physiology and Pharmacology (NPP), Gower Street, University College London, WC1E 6BT, UK

m.beato@ucl.ac.uk

Key words: spinal cord, premotor interneurons, flexor muscles, extensor muscles, rabies, viral tracing

Abstract

The activity of flexor and extensor motor neurons is tightly regulated by a network of interneurons in the spinal cord. The introduction of rabies retrograde monosynaptic tracing has provided a powerful method to map interneurons directly connected to motor neurons so as to visualize premotor circuits. Previous strategies have used AAV for complementing rabies glycoprotein expression in motor neurons to obtain selectivity in transsynaptic transfer to identify premotor interneurons innervating specific motor neuron pools These studies revealed differences in the location of flexor and extensor premotor interneurons. Here, we report that by using a genetic approach to complement rabies glycoprotein expression in motor neurons, we did not observe any differences in the distribution of flexor and extensor premotor interneurons. In order to identify possible causes for these paradoxical findings, we discuss advantages and caveats of the experimental designs and suggest ways forward to resolve possible ambiguities. Furthermore, to obtain a complete picture of existing approaches and results we ask for contributions from the scientific community describing the use of additional mouse models, viral constructs, and complementation methods. The aim is to generate an open, comprehensive database to understand the specific organisation of premotor circuits.

Introduction

Precise regulation in the timing and pattern of activation of muscle groups across a joint is at the basis of motor control. In limbed vertebrates, spinal circuits directing the activity of flexor and extensor muscles are innervated by dedicated pools of motor neurons that receive inputs from different subtypes of excitatory and inhibitory interneurons. Several of these classes of interneurons have been described in electrophysiological, anatomical and genetic studies (Hultborn et al., 1971; Jankowska, 2001; Goulding, 2009), however the incomplete knowledge of the composition of spinal circuits that control the activity of flexor and extensor motor neurons limits progress towards a full understanding of motor circuits.

The introduction of rabies monosynaptic tracing provided a high-throughput method for mapping presynaptic connectivity of selected neuronal populations (Callaway and Luo, 2015). This technique capitalises on the natural ability of rabies virus (RabV) to infect neurons and jump across synapses in the retrograde direction to infect presynaptic neurons. Monosynaptic restriction is achieved by using a mutant virus lacking the gene encoding the rabies glycoprotein (G; ΔG-RabV), which is necessary for transsynaptic transfer, combined with selective complementation of G expression in neurons of choice (Wickersham et al., 2007). Thus, neurons expressing G that are infected with ΔG-RabV becomes “starter cells” from which the virus can jump only one synapse and label selectively presynaptic neurons (Wall et al., 2010; Callaway and Luo, 2015).

Shortly after its introduction, monosynaptic rabies tracing was applied to the study of premotor interneurons in the spinal cord. To obtain selective complementation of G and subsequent rabies monosynaptic transfer from a single motor neuron pool, an elegant approach based on intramuscular co-injection of an AAV expressing G (AAV-G) and ΔG-RabV, both of which can infect motor neurons retrogradely, was described (Stepien et al., 2010). Thus, starter cells are generated in one fell swoop by taking advantage of the stringent anatomical specificity of motor neuron to muscle connectivity (Figure 1A). When this method was applied to study the distribution of premotor interneurons controlling the activity of extensor and flexor muscles in the hindlimb, a prominent spatial segregation along the medio-lateral axis of the dorsal ipsilateral spinal cord was observed, with extensor premotor interneurons found in more medial positions than flexors (Tripodi et al., 2011). More recently, in order to address concerns that this method could also lead to rabies infection and transsynaptic transfer from proprioceptive neurons (Figure 1A; Zampieri et al., 2014), G expression was further restricted to motor neurons by combining the use of a mouse line expressing Cre recombinase under the control of choline acetyltransferase (ChAT) and intramuscular injection of an AAV driving expression of G in a conditional manner (AAV-flex-G; Figure 1B). Under these conditions, segregation of flexor and extensor premotor interneurons was shown at forelimb level (Wang et al., 2017). Finally, a further modification to the original AAV complementation strategy was introduced: stereotactic injection of AAV-flex-G in the spinal cord of *ChAT::Cre* mice was used to target G

expression to cholinergic neurons, with restriction of starter cells to a motor pool achieved by ΔG-RabV muscle injection. These experiments also showed medio-lateral segregation in the distribution of flexor and extensor premotor interneurons (Figure 1C; Takeoka and Arber, 2019). Thus, all the experiments using AAV for complementing G expression in motor neurons demonstrated similar segregation of extensor and flexor premotor interneurons.

We sought to identify premotor interneurons for further investigation, but elected to achieve G complementation by using a mouse genetic approach that takes advantage of a conditional mouse line that drives G expression under control of Cre recombinase (*RΦGT* mice; Figure 1D, 1E; Takatoh et al., 2013). This method has been previously used to trace premotor circuitry of the vibrissal and orofacial motor systems, in combination with *ChAT::Cre* mice (Takatoh et al., 2013; Stanek et al., 2014), and of forelimb muscles in combination with *Olig2::Cre* mice (Skarlatou et al., 2020). We reasoned that using this approach, G should be available at high levels in all motor neurons, thereby leading to efficient monosynaptic transfer from all the cells infected by ΔG-RabV. Surprisingly, in contrast to previous studies, we did not observe any difference in the distribution of flexor and extensor premotor interneurons. The experiments were repeated in different laboratories using different Cre lines, ΔG-RabV preparations, titres and incubation times and all produced similar results. Here, we discuss the advantages and limitations of each method, and propose that the difference in outcome may be due to specific tropism or bias of AAV infection toward a subset of motor neurons within a pool and the possible contribution of disynaptic transfer events. We conclude that more refined approaches, aimed at overcoming the above-mentioned limitations, are needed to resolve the nature of the spatial organization of the premotor network.

Methods

Experimental settings

The experiments were performed and analysed across 4 different laboratories. All the injections on *ChAT::Cre* mice were performed at UCL, either in the Beato or in the Brownstone lab, by 5 different operators. The RabV used was produced at UCL (Beato lab). Tissue preparation and image acquisition were performed either in the Brownstone lab (3 different operators) or at the University of Glasgow (UoG, Maxwell lab, 1 operator). The injections in *Olig2::Cre* mice were performed and analysed at the Max Delbrück Center (MDC), where the RabV was produced.

Animal Experimentation Ethical Approval

All experiments were carried out according to the Animals (Scientific Procedures) Act UK (1986) and were approved by the UCL AWERB committee under project licence number 70/9098. All experiments performed at the MDC were carried out in compliance with the German Animal Welfare Act and approved by the Regional Office for Health and Social Affairs Berlin (LAGeSo).

Mouse strains

Homozygous *ChAT::Cre* mice (Rossi et al., 2011, Jackson lab, stock #006410) or heterozygous *Olig2::Cre* mice (Dessaud et al., 2007) were crossed with homozygous *RΦGT* mice (Jackson Lab, stock #024708), to generate *ChAT::Cre +/-; RΦGT +/-* or *Olig2::Cre +/-; RΦGT +/-* mice (Takatoh et al., 2013; Skarlatou et al., 2020) that were used for rabies tracing experiments. For experiments aimed at distinguishing excitatory and inhibitory populations of premotor interneurons, we crossed homozygous *ChAT::Cre* mice with heterozygous *GlyT2-EGFP* mice (a gift from Prof. Zeilhofer, University of Zurich, Zeilhofer et al., 2005) and their double-positive offspring were mated with the homozygous *RΦGT* mice.

To quantify possible “leak” of Cre expression in the spinal cord, we crossed *ChAT::Cre* and *RCL-tdTom* (Jax Ai9, stock #007909) mice (13 sections from 3 mice), and found tdTom expression in cholinergic motor neurons and interneurons as expected, as well as in some non-cholinergic neurons distributed in intermediate (10%, 70/690) and dorsal (9%, 62/690) laminae, with the remaining 35 located ventrally (see Supplementary figure 1) indicating that ectopic expression of Cre in ChAT negative neurons is minimal but not nil, and mostly confined to superficial dorsal laminae. The possible “leak” of G and the avian receptor protein (TVA) expression in *RΦGT* mice was then tested by injecting EnvA-ΔG-Rab-EGFP, produced according to standard protocols (Osakada and Callaway, 2013) to a titre of 1×10^9 (IU/ml). Lack of contamination from non-pseudotyped virus was confirmed by infecting HEK cells at high (up to 20)

multiplicity of infection. Three *RΦGT* heterozygous mice were injected in the lateral gastrocnemius muscle at P1 and fixed 9 days post injections. The tissue was cut as described below, but along the sagittal plane in 60 µm sections, in order to isolate the dorsal motor column. Following immunoreaction for EGFP, in each of the 3 cords, we found a maximum of 3 labelled motor neurons (1, 1 and 3 motor neurons in n=3 animals) but no interneurons labelled, indicating some leakage in the expression of the TVA-IRES-glycoprotein cassette from the *RΦGT* mice, but insufficient G expression to support trans-synaptic jumps (Supplementary Figure 2).

Virus production

Rabies virus used in experiments performed at UCL, was obtained from in house stocks of a variant of the SAD-B19 rabies strain where the sequence coding for the glycoprotein was replaced by the sequence for either EGFP or mCherry (Wickersham et al., 2007). Virus was produced at high concentration using a the protocol described in (Osakada and Callaway, 2013). Briefly, baby hamster kidney cells stably expressing the rabies glycoprotein (BHK-G, kindly provided by Dr. Tripodi (LMCB, Cambridge) were thawed and plated in standard Dulbecco modified medium, supplemented with 10% fetal bovine serum (FBS), incubated at 37°C with 5% CO_2 and split until ~70% confluence was obtained in 5 dishes (10 ml medium each). The cells were then inoculated at 0.2-0.3 multiplicity of infection with either the ΔG-RabV-EGFP or the ΔG-RabV-mCherry (initial samples kindly provided by Prof. Arber and Dr. Tripodi). Cells were incubated for 6 hours at 35°C and 3% CO_2 and then split 1 to 4 into 20 dishes (10 ml) with 10% FBS medium and kept at 37°C and 5% CO_2 for 12-24 hours, until ~70% confluent. The medium was then replaced with 2% FBS medium and cells incubated at 35°C and 3% CO_2 for virus production. The supernatant was collected after ~3 days, and new medium was added for another round of production. The supernatant was filtered (0.45 µl filter) and centrifuged for 2 hours at 19400 rpm (SW28 Beckman rotor). The pellets were suspended in phosphate buffer saline (PBS), dispersed and collected in a single tube and further centrifuged for 4 hours at 21000 rpm in a 20% sucrose gradient (SW55 Beckman rotor). The resulting pellet was suspended in 100 µl PBS and the virus was aliquoted (5-10 µl) and stored in a -80° freezer. The viral titre of each round of production was measured by serial 10-fold dilution of three different aliquots using standard protocols (Osakada and Callaway, 2013). For each injection, the virus titre is reported in Supplementary Table 1. In a subset of experiments, we diluted the virus 10-fold in order to limit the number of starter cells. Rabies virus used for experiments performed at MDC was produced as previously described (Skarlatou et al., 2020).

Intramuscular injection

Neonatal pups (P1-P2) were anaesthetized using isofluorane inhalation and an incision was made on the skin to expose the belly of the targeted muscle, either lateral or medial gastrocnemius (LG, MG), tibialis

anterior (TA) or peroneus longus (PL). The virus was injected intramuscularly using a 5 µl Hamilton syringe (model 7652-01) fixed to a manual Narishige micromanipulator (M-3333) and loaded with a bevelled glass pipette of inner diameter 50-70 µm. The volume injected was 1 µl, compatible with the estimated volume of the muscles at this age (~2 µl), in order to minimize the risk of leaks to adjacent muscles. Viral batches of similar titres were slowly (> 1 minute) injected at a constant volume of 1 µl. The skin incision was sutured with Vicryl 8-0 (Ethicon, USA) and the pups received a subcutaneous injection of carprofen (10%) for pain management. Mice were closely monitored for the next 24 hours for signs of movement impairment and were perfused 8-9 days after injection.

In order to compare directly the distributions of flexor and extensor associated premotor interneurons and avoid confounding factors in the coordinate representations of these interneurons across different spinal cords, we performed double injections of ΔG-RabV in the same animal, using ΔG-Rab-EGFP and ΔG-Rab-mCherry injected in pairs of antagonist muscles, lateral gastrocnemius and tibialis anterior. For comparison, we also performed double injections in pairs of synergist muscles: LG and MG or TA and PL. Due to the proximity of these pairs of muscles, before cutting the spinal tissue for immunohistochemistry, we dissected the injected leg and confirmed that there was no contamination of virus across the injected muscles or in adjacent muscles below or above the knee. To exclude confounding factors in our observed premotor interneuron distributions due to systematic viral interference (Ohara et al., 2009b, 2009a), in a subset of experiments single injections of ΔG-Rab-mCherry (4 LG, 4 MG, 2 TA and 4 PL) were performed in the progeny of either *ChAT:: Cre;RΦGT* or *GlyT2-EGFP;ChAT::Cre;RΦGT* mice.

For experiments performed at MDC, intramuscular injections were done as previously described (Skarlatou et al., 2020). Briefly, P4 animals were anesthetized with isoflurane and a small incision in the skin was made to reveal either the gastrocnemius (GS, 4 experiments, no attempts were made at selective targeting of the two heads of the GS muscle) or the tibialis anterior (3 experiments) muscles. 1.5 µl of ΔG-RabV-mCherry was injected *in Olig2::Cre +/-; RΦGT +/-* mice using a glass capillary. Animals were euthanized at p10, 6 days after injection in order to minimize the chance of disynaptic transfer.

Tissue collection and immunohistochemistry

Under ketamine/xylazine terminal anaesthesia (i.p. 80 mg/kg and 10 mg/kg respectively), mice were intracardially perfused with phosphate buffer solution (0.1 M PBS), followed by 4% paraformaldehyde in PBS. The spinal cords were dissected and post-fixed for 2 hours at 4ºC, cryoprotected overnight at 4ºC in 30% PBS sucrose solution and embedded in OCT (optimal cutting temperature, Tissue-Tek, #4583) compound.

For UCL experiments, injections were all conducted at UCL, whereas the immunohistochemistry and imaging were conducted on different animals independently in two different laboratories (Maxwell at Glasgow University and Beato/Brownstone at UCL). For experiments performed at UCL, lumbar spinal cords were cut (30 µm thickness) in series in the transverse plane with a cryostat (Bright Instruments, UK) mounted onto charged glass slides (VWR, #631-0108), and stored at -20ºC. Sections were incubated for 36 hours at 4˚C with primary antibodies and overnight at 4˚C with secondary antibodies in PBS double salt solution, 0.2% Triton 100-X (Sigma, T9284-500ml), 7% donkey normal serum (Sigma, D9663-10ml). The primary antibodies used were: guinea pig anti-Isl1 (1:7500, from Dr. T Jessell, Columbia University, New York), goat anti choline acetyl transferase (ChAT, 1:100, Millipore, AB144P), rabbit anti-GFP (1:2500, Abcam. Ab290), chicken anti-mCherry (1:2500, Abcam, Ab205402). The secondary antibodies were: donkey anti-guinea pig Alexa 647 (1:700, Millipore, AP193SA6), donkey anti-goat preabsorbed Alexa 405 (1:200, Abcam, ab175665), donkey anti-rabbit Alexa 488 (1:1000, Thermofisher, A21206), and donkey anti-chicken Cy3 (1:1000, Jackson ImmunoResearch, #703-165-155). The slides were mounted in Mowiol (Sigma, 81381-250G) and cover-slipped (VWR, #631-0147) for imaging.

At Glasgow University, the spinal cords were sectioned using a Leica VT1000 vibratome (thickness 60 µm) and incubated in 50% ethanol for 30 minutes. Primary antibodies used were: chicken anti-GFP (1:1000, Abcam, Ab13970), rabbit anti-mCherry (1:2000, Abcam, Ab167453) and goat anti-ChAT (1:100, Millipore, AB254118). The secondary antibodies were: donkey anti-chicken A488 (1:500, Jackson Immunoresearch, 703-545-155), donkey anti-rabbit Rhodamine red (1:100, Jackson Immunoresearch, 711-295-152) and either Pacific Blue (1:200, prepared on site using unconjugated donkey anti-rabbit IgG, Jackson Immunoresearch, 711-005-152 and Pacific Blue kit, Invitrogen, P30012) or Alexa 647 (1:500, Jackson Immunoresearch, 705-605-003). Sections were mounted in Vectashield (Vector Laboratories, Peterborough, UK) and coverslipped.

For the experiments performed at MDC, spinal cords were processed as previously described (Skarlatou et al., 2020). Briefly, animals were anesthetized by intraperitoneal injection of ketamine /xylazine mix and transcardially perfused with ice-cold PBS until the liver was cleared of blood and followed by freshly made ice-cold 4% PFA. Spinal cords were dissected via vertebrectomy and post-fixed for 90 minutes with 4% PFA on ice. Consecutive 40 µm spinal cord cryosections encompassing the caudal thoracic and lumbar spinal regions were obtained using a Leica cryostat and incubated overnight at 4ºC with rabbit anti-ChAT 1:16000 (Sürmeli et al., 2011 RRID:AB_2750952) followed by 1 hour incubation at room temperature with secondary antibody (Alexa-Fluor 488, 1:1000). Slides were mounted in Vectashield (Vector).

Confocal imaging and analysis

For UCL experiments, confocal images were acquired using a Zeiss LSM800 confocal microscope using a 20X (0.8 NA) air objective and tile advanced set up function of ZEN Blue 2.3 software for imaging of the entire slice. The tiles were stitched using ZEN Blue software and cell detection was performed using Imaris (version up to 9.1, Bitplane) software. Cell counts were manually performed on every other section, in order to minimize the risk of counting the same cell twice in two consecutive sections.

For experiments performed at Glasgow University, the images were acquired using a Zeiss 710, with a x20 air objective and cells were counted manually using Neurolucida. Only a subsample of sections was analysed (1 every 8 consecutive sections), thus accounting for approximately 2 sections for every spinal segment.

A consistent system of coordinates was established using the central canal as origin of the x-y plane and the border between L4 and L5 segments as the origin of the z-axis. The L4-L5 border was determined during the slicing procedure and its location was confirmed post-processing by identifying the slices with the widest mediolateral width. The y-axis was defined as parallel to the dorso-ventral axis, with positive values towards the dorsal side and the x-axis was determined by the mediolateral direction, with positive values on the side of injection. For both Neurolucida and Imaris data files, in order to account for the different shapes of sections throughout the lumbar cord and deformation of individual sections, normalization of coordinates was performed independently for each quadrant using as reference points those indicated in Supplementary Figure 3: the x dimension was normalized to the edge of the white matter at the level of the central canal, while the y dimension was normalized for each quadrant using the outermost points of the white matter for both dorsal and ventral horns. The resulting cylindrical reconstruction of the spinal cord was then scaled to the idealized spinal cord size (1700 μm in the mediolateral direction and 900 μm in the dorsoventral direction) for illustrational purposes. All coordinate transformations were performed using a custom script in MATLAB, adapted to read both Neurolucida and Imaris file formats. Infected motor neurons were identified by co-localization of either Isl1 or ChAT, and the presence of the reporter fluorescent protein (EGFP or mCherry) expressed after rabies infection. Distributions of infected interneurons were calculated using a Gaussian convolution with kernel size calculated from the standard deviation of the original data (Bhumbra and Dyball, 2010).

Gaussian convolutions were calculated splitting the transverse, normalized, spinal cord profile into ipsi- and contra-lateral, and dorsal and ventral halves, with the corresponding distributions shown surrounding the transverse spinal cord maps. Areas under the top-bottom or left-right distributions of each label sum to 1. Correlations across experiments were calculated from the x-y coordinates projected along the rostrocaudal axis by computing a density matrix $\rho_n(x_i, y_i)$ for each experiment n and evaluating the correlation coefficient r_{nm} between experiments n and m using the formula

232 $$r_{nm} = \frac{\sum_i \sum_j (\rho_n(x_i, x_j) - median(\rho_n))(\rho_m(x_i, x_j) - median(\rho_m))}{\sqrt{(\sum_i \sum_j (\rho_n(x_i, x_j) - median(\rho_n))^2)(\sum_i \sum_j (\rho_m(x_i, x_j) - median(\rho_m))^2)}}$$

233 Differences in the mediolateral distribution of premotor interneurons were tested using Wilcoxon rank-sum
234 tests. All data processing was performed in MATLAB, using custom written software (available on request
235 from corresponding authors).

236 For experiments performed at the MDC, confocal images were acquired using a Zeiss LSM800 confocal
237 microscope. Regions of interest corresponding to each section and consisting of 8 tiles were imaged with
238 a 10x air objective. The tiles were subsequently stitched using the ZEN 2.3 Software. Acquisition and
239 processing were performed immediately after immunohistochemistry where applicable to obtain the best
240 possible signal. The resulting images were used for three-dimensional positional analysis as previously
241 described (Skarlatou et al., 2020). Briefly, Cartesian coordinates were obtained using the imaging software
242 IMARIS 9.1. To account for differences in spinal cord size, orientation and shape, the datasets were rotated
243 and normalized against a standardized spinal cord whose size was determined empirically (Medio-lateral:
244 1000 µm, dorso-ventral: 500 µm). To align the datasets along the rostro-caudal axis, the border between
245 T13 and L1 was defined as z=0, and consecutive sections up to 2 mm in the caudal direction were
246 analysed.
247

Results

Flexor and extensor premotor interneurons in ChAT::Cre +/-; RΦGT+/- mice

In order to determine the spatial distribution of premotor interneurons controlling flexion and extension of the ankle, we injected ΔG-RabV/mCherry and ΔG-RabV/GFP in the TA (tibialis anterior; ankle flexor) and LG (lateral gastrocnemious; ankle extensor) muscles of postnatal day (P) 1-2 *ChAT::Cre +/-; RΦGT+/-* mice. Analysis of lumbar level (L) 2 and L5 sections 8-9 days after injection revealed two main clusters of premotor interneurons located in the dorsal ipsilateral and ventral contralateral spinal cord (Figure 2A and 2B) Next, we obtained Cartesian coordinates for the labelled cells in each section of the lumbar spinal cord and mapped premotor interneuron positions in three dimensions. The projection of x-y coordinates along the rostro-caudal axis of the spinal cord showed no difference in medio-lateral and dorso-ventral positions of flexor and extensor premotor interneurons (Figure 2C, left panel). Convolved distributions fully overlapped for the two groups in all four quadrants. Similarly, projection along the sagittal plane (Figure 2C, middle panel) or coronal plane (Figure 2C, right panel) revealed no obvious differences in the rostro-caudal, dorso-ventral and medio-lateral distribution of flexor and extensor premotor interneurons.

Next, to study in detail the positional organization of premotor interneurons controlling the activity of the ankle joint, we analysed 13 animals in which we performed simultaneous ΔG-RabV-EGFP and ΔG-RabV-mCherry injections in 3 different pairs of antagonist and synergist muscles: TA and LG, LG and MG (medial gastrocnemious; ankle extensor and LG synergist) and TA and PL (peroneus longus; ankle flexor and TA synergist). We initially compared a total of 11 LG and 7 TA muscle injections (5 of which were in the same animal. Figure 3A-B). All experiments are overlaid, with different shades of blue (LG) and orange (TA) representing different animals, showing the reproducibility of premotor interneurons distributions across single experiments (pooled distributions shown in Figure 3C, all individual experiments shown separately in figures S5 and S6). In all cases analysed, we did not observe differences in the positional organization of flexor and extensor premotor interneurons. The reproducibility of the results is confirmed by analysis of the positional coordinates across all experiments showing similar correlation values within or across muscles (Figure 3D; $r \geq 0.78$). In order to statistically assess variability in neuronal positioning, we compared the medio-lateral distributions in the dorsal ipsilateral quadrant using a Wilcoxon rank test, and found no statistical difference (median position of pooled LG and TA distributions on the medio-lateral axis were 160 µm and 161 µm respectively, $p=0.42$). The values of the medians of individual experiments for LG and TA injections were normally distributed and not significantly different (Figure 3F; unpaired t-test, $p=0.75$).

Since it was previously shown that the medio-lateral segregation in the distribution of flexor and extensor premotor interneurons is more pronounced in spinal segments rostral to the infected motor nucleus

(Tripodi et al., 2011), we analysed the organization of premotor interneurons at different lumbar levels. Positional coordinates were pooled and divided into 800 µm rostro-caudal bins and distributions were plotted for each bin from L1 to L6 (Figure 4). No significant differences in the medio-lateral distributions of LG and TA premotor interneurons were observed in any segment analysed (median positions on the medio-lateral axis for L1, the segment with the largest visible medio-lateral segregation: LG = 153 µm and TA = 161 µm, p=0.11, Wilcoxon test).

The distribution of premotor interneurons is similar across different pairs of ankle flexors or extensors

Since it has been proposed that medio-lateral segregation of premotor interneurons is a general feature of flexor and extensor muscles, we analysed premotor interneurons of two more muscles controlling the movement of the ankle joint, PL and MG. The distributions of premotor interneurons of LG (6 LG-MG injections, 8 LG-TA injections and 4 single LG injections) and MG (6 LG-MG injections and 4 MG injections) did not reveal any difference in spatial organization (median value of the medio-lateral position of the pooled distribution was 157 µm for LG and 153 µm for MG, Figure 5A), regardless of the infection efficiency. The positions of rabies-labelled neurons were highly correlated (Figure 5B, $r \geq 0.74$) and reproducible along the medio-lateral axis (Figure 5C), with median values not significantly different (Figure 6D; unpaired Student's t-test p=0.74). The same result was observed for TA and PL premotor interneurons (Figure 5E; 2 TA-PL injections, 8 TA-LG injections, 2 TA single injections and 3 PL single injections), where the median of the mediolateral pooled distributions were 158 µm for TA and 168 µm for PL, with high correlation values between experiments (Figure 5F; $r \geq 0.66$), similar medio-lateral distributions (Figure 5G), and median values (Figure 5H; unpaired Student's t-test p=0.15). Together, these data show that premotor interneuron maps obtained using ΔG-RabV muscle injection in *ChAT::Cre +/-; RΦGT+/-* mice do not reveal any difference in the positional organization of interneurons controlling the activity of the main flexor and extensor muscles of the ankle.

The identity of infected motor neurons

The identity of starter cells represents a critical element for the interpretation of rabies tracing experiments. In our and others' approaches, it is difficult to unambiguously determine the identity of starter motor neurons since the complementation of G is not accompanied by the expression of a reporter gene. In addition, a precise estimation of the total number of infected motor neurons is complicated by rabies toxicity that kills many neurons shortly after infection (Reardon et al., 2016). Nevertheless, we took advantage of the topographic organization of motor neuron to muscle connectivity to evaluate the pool identity and number of infected motor neurons that survived until the end of the experiment (Romanes, 1964; McHanwell and Biscoe, 1981). As predicted by the known position of the TA and LG motor pools in the

spinal cord, we found that the majority of infected motor neurons were localized in the dorsal part of the ventral horn (Figure 2C; Sürmeli et al., 2011). Surprisingly, we also found motor neurons in more ventral, "ectopic" positions (Figure 2C and Figures S5-S9), where pools that innervate muscles controlling the function of the knee and hip joints reside (Sürmeli et al., 2011). Motor neuron labelling occasionally extended outside the lower lumbar segments where most of the ankle flexors and extensor pools are located (Figures S5-S9). Moreover, in double TA and LG injections we found instances of motor neurons infected with both viruses (Figures 2D and 2E). In 5 experiments, a total of 200 LG and 150 TA motor neurons were labelled, of which 13 were infected with both ΔG-RabV-EGFP and ΔG-RabV-mCherry (see Table 1).

The presence of ectopic and double labelled motor neurons could be explained by either secondary labelling due to rabies transsynaptic transfer from starter cells through recurrent connections onto other motor neurons or by unintended primary infection of motor neurons due to non-specific muscle injections. Careful post-hoc analysis of hindlimb muscles after ΔG-RabV injection did not reveal any evidence of non-specific muscle infection. In addition, it is unlikely that the relatively small volume of ΔG-RabV solution used in the experiments would lead to spread to other muscles, particularly those located in compartments on the other side of the bone or joint, where muscle targets of the ectopic motor neurons reside. We therefore suggest that ectopic motor neurons were mostly labelled by transsynaptic labelling and therefore represent second-order presynaptic neurons. This is not surprising, as motor neurons have been shown to form synapses with other motor neurons and that their connections can extend to neighbouring spinal segments. In addition, paired recordings from retrogradely labelled motor neurons have revealed that not only motor neurons belonging to the same nucleus (Bhumbra and Beato, 2018), but also antagonist motor neurons are reciprocally connected in mice (Özyurt et al., unpublished data). These data suggest that the ectopic motor neurons found in our experiments were most likely due to rabies transsynaptic transfer. Regardless of the underlying reasons for the observed ectopic motor neuron labelling, its presence raises the possibility that what we defined as flexor and extensor premotor networks, might, in fact, originate from a mixed population of starter cells containing not only motor neurons of a single pool identity but also a fraction of , "non-specific", motor neurons belonging to other pools, thereby potentially diluting any observable spatial difference between the premotor networks of flexor and extensor muscles. However, it is important to notice that in our experiments the number of presumed "non-specific" starter cells is low and unlikely to confound the results (Table 1; see below and Discussion).

The number of infected motor neurons does not affect the distribution of premotor interneurons

Spinal or muscle injection of AAV to complement G expression is likely to result in infection of a subset of motor neurons within the targeted pool, whereas the genetic experiments will result in complementation in all motor neurons. Thus, it is possible that the difference in the results obtained with these two methods

may lie in the absolute number of motor neurons from which rabies synaptic transfer occurs. In order to test the effect of the number of starter cells in our experimental conditions, we reasoned that by reducing the viral titre of the rabies solution used for muscle injection, we would scale down the number of infected motor neurons. Therefore, we performed a series of muscle injections (7 LG and 6 TA, of which 3 double LG-TA) with diluted rabies virus (titre $<10^9$ I.U./ml) to reduce its infection efficiency (see Table 1). In low titre experiments, we detected an average 4.7 infected motor neurons compared to an average of 35.2 in the high titre experiments (titre $>5\times10^9$ I.U./ml). Once again, we did not observe segregation in the medio-lateral distribution of LG and TA premotor interneurons (Figures 6A-C). While there was a higher degree of variability between experiments compared to high titre injections, as shown in the correlation matrix of individual experiments (Figure 6D, r>0.45 for all comparisons), the median value of the medio-lateral position of the pooled distributions (LG = 153 µm and TA = 161 µm, p=0.2, Wilcoxon rank test), as well as the medians of individual experiments, were not significantly different (p=0.43, unpaired t-test; Figure 6E, F, individual experiments shown in Figures S10,11,12). Next, we compared high and low titre experiments for each muscle injected (Figure S4). The distribution of premotor interneurons shows remarkable overlap for both LG and TA injections (Figure S4A and S4D). The medio-lateral distributions were not significantly different for LG (medians: high = 153 µm and low = 154 µm, p=0.19, Wilcoxon rank test) and only slightly shifted in the lateral direction for low titre injections into TA (medians: high = 151 µm and low = 162 µm, p=0.03, Wilcoxon rank test). Of note, in low titre experiments we never observed ectopic motor neurons outside the expected nucleus (Figures S10, 11,12). Together, these data indicate that neither the absolute number of starter motor neurons nor the infection of ectopic motor neurons observed in high titre experiments significantly affects the positional organization of premotor interneurons.

Flexor and extensor premotor interneurons tracing in Olig2::Cre +/-; RΦGT+/- mice

An important consideration concerning the use of our genetic approach for G complementation is the expression specificity of the Cre driver: recombination in multiple neuronal subtypes can potentially result in loss of monosynaptic restriction and rabies transfer across multiple synapses (Figure 1D and E). In the spinal cord, *ChAT::Cre* is not only expressed in motor neurons but also cholinergic interneurons, including medial partition cells (V0c neurons) that have prominent projections to motor neurons (Zagoraiou et al., 2009). Therefore, given that under our experimental conditions, V0c neurons express G and are presynaptic to motor neurons, they could permit disynaptic rabies transfer: first from motor neurons to V0c neurons and second from V0c neurons to their presynaptic partners. However, it is important to note that V0c presynaptic partners have been previously characterised using rabies monosynaptic tracing and comprise mostly interneurons located in the dorsal laminae of the spinal cord (Zampieri et al., 2014), an area that is largely devoid of rabies labelling in our experiments as well as in AAV-based experiments (Stepien et al., 2010; Tripodi et al., 2011).

In order to test whether disynaptic transfer from premotor interneurons is affecting our analysis, we performed a set of experiments (4 gastrocnemious, GS and 3 TA injections) using the *Olig2::Cre* (Dessaud et al., 2007) instead the *ChAT::Cre* line. This line would ensure recombination in motor neurons but not in V0c or other cholinergic interneurons. However, Olig2 is also transiently express during embryonic development in subsets of p2 and p3 progenitors (Chen et al., 2011). We reasoned that if additional transsynaptic transfer from premotor interneurons is significantly affecting our results, using a different Cre line to drive G expression in a non-overlapping subset of premotor interneurons should result in different labeling patterns. We performed monosynaptic tracing experiments after single injections of ΔG-RabV/mCherry in either the TA or GS muscles of P4 *Olig2::Cre +/-; RΦGT+/-* mice and analysed the lumbar spinal cord six days later. We did not observe any difference in the positional organization of flexor and extensor premotor interneurons (Figures 7A-E, S15, and S16). Comparison of the premotor maps obtained from *ChAT::Cre* and *Olig2::Cre* experiments showed that interneuron distributions were indistinguishable, as shown by the high correlation values across mouse lines and muscles (Figure 7F, r>0.9). In addition, the median interneuron positions along the medio-lateral axis for each experiment were not significantly different between *ChAT::Cre* (157 µm for GS and 154 µm for TA) and *Olig2::Cre* (140 µm for GS and 146 µm for TA) animals injected in the same muscle (Figure 7G, p=0.1 and 0.4 for LG and TA pairs respectively, Wilcoxon test). Thus, these results indicate that under our experimental conditions the results of tracing experiments done in *ChAT::Cre +/-; RΦGT+/- and Olig2::Cre +/-; RΦGT+/-* mice are unlikely to be influenced by disynaptic rabies transfer from spinal premotor interneurons.

Spatial distribution of excitatory and inhibitory premotor interneurons

Next, we examined whether there are differences in the spatial organization of excitatory vs inhibitory premotor interneurons. We performed single LG or TA injections of ΔG-RabV/mCherry in *ChAT::Cre +/-; RΦGT+/-* mice carrying an allele expressing GFP under the control of the neuronal glycine transporter (GlyT2; Zeilhofer et al., 2005). Since a large overlap in the expression of GlyT2 and GABA has been shown in the spinal cord, GlyT2^{on} interneurons can be roughly categorised as inhibitory, while GlyT2^{off} neurons as excitatory (Todd and Sullivan, 1990; Todd et al., 1996).

We first compared the distribution of excitatory (Figure 8A-C) interneurons that are premotor to LG and TA motor neurons, and then did the same for inhibitory (Figure 8D-F) interneurons. The distribution of GlyT2^{off} premotor interneurons were the same for LG and TA motor neurons (4 LG and 3 TA single injections, Figure 8A). The medians of the medio-lateral position in the dorsal ipsilateral cord were 151 µm and 161 µm for LG and TA respectively (p=0.23, Wilcoxon test) and -60 µm and -34 µm (p=0.4, Wilcoxon test) in the ventral spinal cord (Figure 8B and 8C). Similarly, we did not observe segregation in the distribution of GlyT2^{on} LG and TA premotor interneurons (Figure 8D). The medians of the medio-lateral coordinates of

the dorsal GlyT2^{on} interneurons were 152 µm for LG and 173 µm for TA (p=0.06, Wilcoxon test), while for ventral interneurons were 195 µm for LG and 216 µm for TA (p=0.06, Wilcoxon test, Figure 8E, 8F). High correlation values (r>0.79). between all individual experiments underscored the conserved positional organization of LG and TA premotor interneurons. Thus, these data indicate that there is no significant difference in the distribution of putative excitatory or inhibitory premotor interneurons controlling the activity of flexor and extensor muscles.

Finally, we compared the distributions of excitatory and inhibitory premotor interneurons that are presynaptic to LG (Figure 8G-I) and then to TA (Figure 8J-L) motor neurons. No differences were observed for the medio-lateral distribution of inhibitory and excitatory dorsal premotor interneurons (medians for LG: GlyT2^{on} = 151 µm and GlyT2^{off} = 153 µm; p=0.9. Medians for TA: GlyT2^{on} = 161 and GlyT2^{off} = 170 µm; p=0.4). In contrast, ventral ipsilateral GlyT2^{on} were more abundant than GlyT2^{off} for both LG (Figure 8H and 8I) and TA (Figure 8K and 8L). Conversely, GlyT2^{off} premotor interneurons dominated the ventral contralateral side (Figure 8H and 8K; medians for LG: GlyT2^{off} = -61 µm and GlyT2^{on} = 195 µm; p=10^{-38}, Wilcoxon test. Medians for TA: GlyT2^{off} = 37 µm and GlyT2^{on} = 216 µm; p=10^{-26}, Wilcoxon test). Overall, the data show a clear segregation in the distributions of excitatory and inhibitory premotor interneurons in the ventral half of the spinal cord: GlyT2^{on} inhibitory interneurons are almost exclusively found in the ipsilateral side while GlyT2^{off} excitatory interneurons also present a prominent peak in the contralateral side (Figure 8G-K). These observations are reflected in the overall low correlation value in the position of excitatory and inhibitory premotor interneurons for both LG and TA premotor interneurons ($r \leq 0.4$).

Taken together, these findings indicate that while we are able to detect significant differences in the positional organization of premotor interneurons, such as seen in the distribution of excitatory and inhibitory interneurons, we still fail to detect differences when comparing the distributions of flexor and extensor premotor circuits.

Discussion

Spinal circuits are responsible for integrating descending commands and sensory information to ensure precise control and coordination of movement. In order to understand how these circuits organise movement, it is necessary to first identify and then study the roles and contributions of the spinal interneurons that control the activity of different muscles. Previous work exploited rabies monosynaptic tracing to examine the organization of spinal interneurons controlling the activity of selected muscle. These studies, using intramuscular injection of an AAV expressing the rabies glycoprotein G, identified clear segregation in the spatial organization of premotor circuits directing the activity of flexor and extensor muscles (Tripodi et al., 2011; Wang et al., 2017; Takeoka and Arber, 2019). We report here that by genetically complementing G expression, no differences in the distribution of flexor and extensor premotor interneurons was observed. We discuss similarities, differences, and possible caveats, in an attempt to understand the reasons behind contrasting results obtained using these two methods.

AAV- based strategies for rabies monosynaptic tracing of premotor circuits

In previous studies in which segregation of flexor and extensor premotor interneurons has been observed, AAV was used to express G in motor neurons. In the first report, AAV-G and ΔG-RabV are co-injected intramuscularly in wild type mice (Tripodi et al., 2011). This approach has the advantage of complementing G only in motor neurons projecting to the targeted muscle, thus avoiding the problem of G expression in spinal interneurons that could lead to loss of monosynaptic restriction. However, since sensory neurons in the dorsal root ganglia also innervate muscles, such strategy could lead to anterograde transsynaptic spread to the spinal cord through the sensory route (Figure 1A, Zampieri et al., 2014). In order to avoid this problem, intramuscular co-injection of a conditional AAV vector (AAV-flex-G) with ΔG-RabV in *ChAT::Cre* mice was used (Figure 1B, Wang et al., 2017). In this more stringent condition, G would only be expressed in motor neurons. And a more recent study used intraspinal injection of AAV-flex-G in *ChAT::Cre* mice (Figure 1C, Takeoka and Arber, 2019). Using these latter two methods avoids transfer from sensory neurons, but intraspinal delivery of AAV-flex-G can transduce G expression in other cholinergic spinal neurons, thus potentially resulting in rabies disynaptic transfer. However, despite the fact that these AAV-based strategies have distinct advantages and disadvantages, they all faithfully result in labelling of flexor and extensor premotor interneurons with distributions that are medio-laterally segregated in the dorsal ipsilateral quadrant of the spinal cord (Tripodi et al., 2011; Wang et al., 2017; Takeoka and Arber, 2019). Altogether these results indicate that potential transfer from either sensory neurons or cholinergic interneurons does not significantly affect the results obtained in AAV-based rabies tracing experiments.

Mouse genetic-based strategies for rabies monosynaptic tracing of premotor circuits

We opted for a mouse genetic strategy that was previously used to trace premotor circuits of vibrissal, orofacial, and forelimb muscles (Takatoh et al., 2013; Stanek et al., 2014; Skarlatou et al., 2020). Combining a conditional allele expressing G from the rosa locus (*RΦGT* mice; Takatoh et al., 2013) with either the *ChAT::Cre* or *Olig2::Cre* lines (Figure 1D-E) is predicted to result in robust G expression in all motor neurons at the time of rabies muscle injection and therefore in robust transsynaptic transfer. Indeed, under these conditions, several hundred premotor neurons can be reproducibly traced in each experiment (Table 1; Skarlatou et al., 2020). On the other hand, this strategy suffers from the undesirable consequences of lineage tracing, namely G complementation in all Cre expressing cells in the spinal cord, including those that transiently activate the targeted promoter during development. This problem is in part shared with the AAV-based experiments using intraspinal injection of AAV-flex-G in *ChAT::Cre* mice (Takeoka and Arber, 2019). Thus, it is unlikely that the differences in the results obtained using these two strategies was caused by disynaptic transfer through cholinergic interneurons. Indeed, work using rabies monosynaptic tracing to identify spinal neurons presynaptic to the most prominent population of premotor cholinergic interneurons, V0c neurons, found that pre-V0c neurons are for the most part located in superficial laminae of the dorsal horn (Zampieri et al., 2014), an area where no labelling was observed in both AAV- and mouse genetic-based experiments.

Nonetheless, to further explore the possibility of disynaptic pathways via cholinergic spinal interneurons, we examined flexor and extensor premotor circuits in *Olig2::Cre +/-; RΦGT+/-* line. Olig2 is expressed in motor neurons and in subsets of p2 and p3 progenitors, thus potentially generating opportunities for dysinaptic transfer through V2 and V3 premotor interneurons (Chen et al., 2011). We did not find any significant difference in the distribution of premotor interneurons obtained in these mice compared to those in *ChAT::Cre+/-; RΦGT+/-* mice. Therefore, it appears that disynaptic transfer is not a frequent event in our experimental conditions; otherwise, neuronal labelling in *ChAT::Cre* experiments would reflect the contribution of cholinergic interneurons, and *Olig2::Cre* experiments would reflect jumps through V2 and V3 interneurons.

It is also important to consider the timing of rabies transsynaptic transfer (Ugolini, 2011). The earliest expression of rabies in primary infected motor neurons is first observed 3-4 days after injection and monosynaptic transfer not earlier than 5 days after injection, with strong labelling observed around 7-8 days. Since in our experiments, mice were sacrificed between 6 to 9 days following RabV injections (8-9 days in *ChAT::Cre* and 6 days in *Olig2::Cre* mice), it is unlikely that many, if any, double jumps would have occurred in this time window.

Together, these considerations indicate that contamination of premotor circuit maps with interneurons labelled from transsynaptic transfer events originating from G expressing spinal interneurons is not likely to be the source of the different results obtained in AAV and mouse genetic experiments.

The issue of starter motor neurons

The identity and number of starter cells are the main determinants of reproducibility in rabies tracing experiments and thus represent key parameters for comparing different approaches. For experiments using ΔG-RabV, starter cells are those that are both primarily infected with RabV and express G. In general, for both the AAV and mouse genetics methods discussed here, it is difficult to precisely determine these factors, as neither approach employs expression of a reporter gene to mark G-expressing cells. Moreover, rabies is known to be toxic to neurons and a proportion of primary infected motor neurons is likely to die before analysis (Reardon et al., 2016). Because of the well-known topographic organization of neuromuscular maps, muscle identity of infected motor neurons can be inferred by their stereotyped position in the spinal cord (Romanes, 1964; McHanwell and Biscoe, 1981). Thus, for all the methodologies discussed here, it is only possible to approximate the identity and number of starter motor neurons by surveying the position of rabies infected motor neurons present at the end of the experiment.

Restriction of starter “status” to motor neurons connected to a single muscle is determined by two aspects: the specificity of rabies virus injection and the availability of sufficient levels of G protein in the same cells (Callaway and Luo, 2015). All the approaches discussed here used intramuscular injections of G-deleted rabies virus (SAD-B19) to selectively infect a motor pool. In this step, sources of variability are represented by 1) specificity of muscle injection and 2) the titre of the rabies virus injected. Muscle injections specificity was routinely checked for injections of adjacent synergist muscles. Rabies leak from antagonist muscles (LG and TA) located on opposite sides of the tibia and fibula, especially at the low volumes used in this study, would be very unlikely. The titre of the injected rabies virus can affect the efficiency of primary infection: the data presented here show that the RabV titre, while affecting the number of motor neurons and secondary neurons labelled, does not change the overall distribution of premotor interneurons. The same data indicate that the presence of a small number of ectopic motor neurons does not significantly contribute to the tracing results, as the premotor distributions in high and low titre experiments are not different despite the presence of ectopic motor neurons in high titre injections. In addition, because of motor neuron recurrent connectivity, the majority of ectopic cells likely represent second-order presynaptic motor neurons (Bhumbra and Beato, 2018), therefore any labelling originating from them would represent a much less frequent disynaptic transfer event.

The AAV- and genetic-based approaches arguably differ the most in regards to the expression of the G glycoprotein in motor neurons. The use of either *ChAT::Cre* or *Olig2::Cre*, to excise the stop cassette in

the *RΦGT* allele is expected to drive G expression in all motor neurons because of their cholinergic nature or because of Olig2 expression at progenitor stage. Conversely, the use of AAV is likely to transduce expression of G only in a subset of motor neurons within a pool (Li et al., 2008; Towne et al., 2010). In addition, since viruses naturally differ in their ability to infect different cell types (Castle et al., 2016), it is possible that AAV may display a preference towards a particular motor neuron subtype. It is currently unclear whether the AAV serotype (2.6) used for premotor tracing experiments exhibits tropism for a particular population of motor neurons. Motor pools are not homogeneous: they can be divided based on molecular and functional properties into three major classes alpha, beta, and gamma motor neurons (Manuel and Zytnicki, 2019). In addition, pools contain different types of alpha-motor neurons, whose intrinsic properties are specifically tuned to the contractile properties of the muscle fibers they innervate and can thus be further sub-classified into three distinct subtypes (S, FR, and FF; Manuel and Zytnicki, 2019). Thus, preferential AAV infection toward a specific motor neuron class and/or subtype may provide the solution for interpreting the results obtained with AAV-based and genetic-based experiments. And it is intriguing that premotor interneurons to a particular subtype of motor neuron may be segregated. To fully understand the differential results, it would be useful in future experiments to precisely determine the identity of starter motor neurons to clarify whether preferential expression of G in a specific motor neuron class could result in mapping a spatially-restricted subset of premotor interneurons.

In the short term, the introduction of a reporter system to label G expressing neurons, as routinely done in many rabies experiments, combined with the use of non-toxic rabies variants that would prevent motor neuron death (Reardon et al., 2016; Ciabatti et al., 2017; Chatterjee et al., 2018) will help resolve potential confusion about the identity and number of starter cells. Such tools could be used in both the AAV and the mouse genetic approaches. In addition, the ability to precisely restrict the selection of starter motor neurons either by the introduction of more specific Cre lines or the use of novel intersectional genetic and viral strategies would improve to design of premotor tracing experiments. Finally, tracing from single motor neurons using delivery of DNA for G and TVA expression via patch clamp is a very precise way to generate specific starter cells (Marshel et al., 2010; Rancz et al., 2011). This approach, followed by intraspinal injection of EnVA-pseudotyoped ΔG-RabV, would ensure infection and pre-synaptic tracing from only selected neurons (Figure 1F). While technically challenging, this method would have the added value of directly showing whether functionally distinct motor neurons within a pool receive differentially distributed presynaptic input.

Conclusions

In conclusion, it is important to stress that none of the methods discussed here is completely exempt from potential problems (Table 2). However, full appreciation of the strengths and weaknesses of each

approach can guide both the choice of method for mapping premotor circuits and the interpretation of the results obtained. The importance of resolving these apparently contrasting results regarding the organization of flexor and extensor premotor circuit leads us to appeal to other laboratories who have performed similar experiments to share their data. Comprehensive comparison of all available protocols and results would lead to the optimisation of new methodologies and contribute to our understanding of spinal motor circuits.

Acknowledgements

This work was supported by a BBSRC grant to MB, AJT and DJM (grant number BB/L001454), a Leverhulme Trust grant to MB (grant number RPG-2013-176) and a Wellcome Trust Investigator Award to RMB (110193). RMB is supported by Brain Research UK. SS and NZ were supported by the DFG (ZA 885/1-1 and EXC 257 NeuroCure). We are extremely grateful to Dr. Marco Tripodi and Professor Silvia Arber for constructive discussions during the preparation of this manuscript and for their helpful comments to the text.

Figure legends

Figure 1. Schematic diagram of the currently available techniques for labelling premotor interneurons. A: simultaneous injection of RabV and AAV-G into muscles. Rabies transfer pathways that could potentially contaminate the distribution of premotor interneurons are labelled by a question mark and indicated by dashed lines. A: Afferent labelling could lead to anterograde labelling of sensory related interneurons. B: simultaneous muscle injection of RabV and a Cre dependent AAV-G into mice expressing Cre in motor neurons eliminates the risk of anterograde transfer from afferents. C: intraspinal injection of a flexed AAV-G in mice expressing Cre in motor neurons is followed by intramuscular rabies injection. D and E: RabV muscle injection is performed on mice selectively expressing the rabies glycoprotein in cholinergic neurons (D) or neuron expressing the Olig2 transcription factor (E). F: a single motoneuron is patched and infected through the patch pipette with viruses coding for a fluorescent reporter (tdTom), the RabV glycoprotein and the TVA receptor. Following expression of the constructs, spinal injection of EnvA-ΔG-Rab-GFP will give rise to infection of a single motor neuron and the tracing of its synaptic contacts, providing a unambiguous identification of the starter cell and its presynaptic partners.

Figure 2. Double injections of flexor and extensor muscles shows no segregation of premotor interneurons. A: Maximum intensity projection of a single 30 µm section taken from the L2 segment of a P10 cord infected with ΔG-Rab-mCherry in the LG and ΔG-Rab-EGFP in the TA in ChAT-*RΦGT* mice. B: Same experiment as A, showing a L5 section. C: Projections along the transverse (left), sagittal (middle) and coronal (right) axes throughout the lumbar region. Dots denote individual premotor interneurons, triangles denote infected motor neurons. Convolved density along each axe are shown to the sides of the raw data (top-bottom and left-right distributions in all panels sum to 1). D: Half section of a cord on the side of a double injection of LG and TA in the L4 segment. Some isl1+ motor neurons are labelled in the dorsal nuclei and one (indicated by arrowhead and enlarged in E) is labelled by both fluorescent proteins, indicating a potential trans-synaptic jump between antagonist motor neurons (scale bars, 250 µm and 50 µm in D and E respectively).

Figure 3. Consistent distribution of flexor and extensor premotor interneurons across all individual experiments. A, B: Distribution of premotor interneurons of LG (A) and TA (B) for all the injections. Distributions for each individual experiment are represented with different shades of blue and orange. C: All experiments (single or double ΔG-RabV injections) pooled, showing an overlap of the flexor and extensor related distribution in all quadrants of the spinal cord, with individual dots replaced by contours. D: Correlation across all pairs of experiments, indicating a high degree of consistency across all animals, independent of the muscle injected. E: Box and whisker plot of the mediolateral position of dorsal ipsilateral premotor interneurons in each experiment. F: Values of the median for each LG and TA experiment.

Figure 4. The distribution of premotor interneurons is similar throughout the lumbar spinal cord: data pooled from 18 experiments (11 LG and 7 TA injections) show that within each lumbar segment, from L1 to L6, the distributions of LG and TA premotor interneurons are overlapping.

Figure 5. Pairs of flexor or extensor muscles show similar distributions of premotor interneurons. A, comparison of pooled data from extensor muscles LG and MG injections. B: correlation coefficients across all experiments. C: box and whisker plots of the mediolateral position of dorsal ipsilateral premotor interneurons for each experiment and distribution of median values (D). E: similar plot as A, showing the distribution of premotor interneurons following injections of the flexor muscles TA and PL. Correlations across each experiment are shown in F. G and H shows the mediolateral distribution and the position of the median for each experiment, respectively.

Figure 6: Injection with diluted RabV do not reveal any segregation between flexor and extensor premotor interneurons. A and B show the distribution of LG and TA premotor interneurons on the transverse plane for individual experiments, represented with different colour shades. C: LG and TA distributions overlap and the premotor interneuron distributions are highly correlated across experiments (D). E: Box and whisker plot of the mediolateral position of dorsal premotor interneurons in each experiment. F: Values of the median for each LG and TA experiment.

Figure 7: The distribution of flexor and extensor premotor INs is similar in *Olig2::Cre; RΦGT*. A, B: Single lumbar sections form animals injected in the GS (A) or TA (B) muscles. C - E: Overlay of individual GS (C) and TA (D) experiments and pooled experiments (E). F: Correlation coefficients (minimum value 0.953) between injections of different muscles and using a different driver for Cre expression. G: Box and whisker plots of median values of all the medio-lateral distributions.

Figure 8: GlyT2^{on} and GlyT2^{off} premotor interneurons are distributed similarly for TA and LG. A, B: Distribution of GlyT2^{off} (A) and GlyT2^{on} (D) premotor interneurons following LG and TA injections pooled from 4 LG and 3 TA experiments in *GlyT2-EGFP::ChAT-Cre* mice crossed with RΦGT mice, indicating that neither class of premotor interneurons is segregated across muscles. Boxplots and violin plots (B for GlyT2^{off} and E for GlyT2^{on}) show uniformity of distribution across experiments in both the dorsal (top) and ventral (bottom) halves of the cord. C (GlyT2^{off}) and F (GlyT2^{on}) show boxplots and individual values for the medians of the mediolateral distributions restricted to dorsal (top) or ventral (bottom) part of the cord. Ventral premotor GlyT2^{off} and GlyT2^{on} interneurons are differentially distributed. Comparison of excitatory and inhibitory premotor interneurons in LG (G) and TA (J) muscles are similar in the dorsal cord, but differ in the ventral cord, where most ipsilateral premotor interneurons are GlyT2^{on}, and the majority of

652 contralateral premotor interneurons are GlyT2^{off}. Boxplots and violin plots of individual experiments are
653 shown in H for LG and K for TA, highlighting the mediolateral differences in the ventral cord. The medians
654 of the ventral and dorsal distributions are shown in I for LG and L for TA.
655

Supplementary figure legends

Supplementary Figure 1: Analysis of ectopic Cre expression in *ChAT-IRES-Cre* and *RCL-tdTom* mice. A: representative lumbar section stained with antibodies against ChAT (green) and tdTom (red) and (B) map of neurons labelled with both or one of the two antibodies in all the 13 analysed sections from 3 mice, showing that some of the tdTom positive neurons do not express ChAT, indicating either a developmental downregulation of ChAT expression or a modest leak in the Cre expression. C: Venn diagram showing the overall number of mapped neurons.

Supplementary Figure 2: Two examples of a longitudinal section of two different spinal cords from a heterozygous *RΦGT* mouse injected in the LG with EnvA-ΔG-Rab-EGFP, showing a small number of infected motor neurons, but no evidence of transsynaptic jumps, indicating ectopic expression of the TVA receptor, but not of the rabies glycoprotein.

Supplementary Figure 3. Schematic of a section of the spinal cord, indicating the reference points used for normalization. Each section was translated to have the origin of a Cartesian set of axes centered on the central canal (CC). A line passing through the central canal and perpendicular to the dorso-ventral axis was used to identify the edge of the white matter in the mediolateral direction (ml) and the ml-CC distance was used to normalize the x-coordinates. Along the dorso-ventral axes, the 4 edges of the white matter (ne, nw, se, sw) were identified and their distance from the horizontal line passing through the central canal were used to normalize the y-coordinates independently in each of the 4 quadrants.

Supplementary Figure 4: High and low efficiency infections give rise to the same premotor interneurons distributions. Comparison of high and low titre injections are shown in A and D for LG and TA respectively. The distributions are similar across experiments for both muscles (B and E) and the median values of the distributions in the ipsilateral dorsal quadrant are not different for high and low efficiency of infection (C and F)

Supplementary Figure 5: Representation of individual experiments (LG and TA double injections in *ChAT::Cre; RΦGT* mice) obtained at UCL. Same experiment code as Table 1. Individual dots denote premotor interneurons, triangles denote infected motor neurons.

Supplementary Figure 6: Representation of individual experiments (LG and TA double injections in *ChAT::Cre; RΦGT* mice) obtained at University of Glasgow. Same experiment code as in Table 1. Individual dots denote premotor interneurons, triangles denote infected motor neurons.

Supplementary Figure 7: Representation of individual experiments (LG and MG, double injections in *ChAT::Cre; RΦGT* mice) obtained at UCL. Same experiment code as in Table 1. Individual dots denote premotor interneurons, triangles denote infected motor neurons.

Supplementary Figure 8: Representation of individual experiments (LG and MG, double injections in *ChAT::Cre; RΦGT* mice) obtained at University of Glasgow. Same experiment code as in Table 1. Individual dots denote premotor interneurons, triangles denote infected motor neurons.

Supplementary Figure 9: Representation of individual experiments (TA and PL, double injections in *ChAT::Cre; RΦGT* mice) obtained at UCL. Same experiment code as in Table 1. Individual dots denote premotor interneurons, triangles denote infected motor neurons.

Supplementary Figure 10: Representation of individual experiments (LG and TA double injections in *ChAT::Cre; RΦGT* mice) obtained at University of Glasgow using a diluted RabV (titre $<10^9$ I.U./ml Same experiment code as in Table 1. Individual dots denote premotor interneurons, triangles denote infected motor neurons.

Supplementary Figure 11: Representation of individual experiments (LG single injections in *ChAT::Cre; RΦGT* mice) obtained at University of Glasgow. Same experiment code as in Table 1. Individual dots denote premotor interneurons, triangles denote infected motor neurons.

Supplementary Figure 12: Representation of individual experiments (MG single injections in *ChAT::Cre; RΦGT* mice) obtained at University of Glasgow. Same experiment code as in Table 1. Individual dots denote premotor interneurons, triangles denote infected motor neurons.

Supplementary Figure 13: Representation of individual experiments (TA single injections in *ChAT::Cre; RΦGT* mice) obtained at University of Glasgow. Same experiment code as in Table 1. Individual dots denote premotor interneurons, triangles denote infected motor neurons.

Supplementary Figure 14: Representation of individual experiments (PL single injections in *ChAT::Cre; RΦGT* mice) obtained at University of Glasgow. Same experiment code as in Table 1. Individual dots denote premotor interneurons, triangles denote infected motor neurons.

Supplementary Figure 15: Representation of individual experiments (GS, single injections in *Olig2::Cre; RΦGT* mice) obtained at Max Delbrück Center. Same experiment code as in Table 1. Individual dots denote premotor interneurons, triangles denote infected motor neurons.

Supplementary Figure 16: Representation of individual experiments (TA, single injections in *Olig2::Cre; RΦGT* mice) obtained at Max Delbrück Center. Same experiment code as in Table 1. Individual dots denote premotor interneurons, triangles denote infected motor neurons.

730

Table 1

Code	Lab	Injection	Perfusion	Muscle	Titre I.U.	MNs	Double labelled MNs	Ipsi premotor INs	Contra premotor INs	Total premotor INs	premotor INs/MNs ratio	Section sampling
170427n2	UCL	P2	P10	LG	1×10^{10}	46	3	741	116	857	19	1/2 (30 µm)
				TA	5×10^{9}	41		912	88	1000	24	
170427n3	UCL	P2	P10	LG	1×10^{10}	32	2	620	87	707	22	1/2 (30 µm)
				TA	5×10^{9}	6		386	34	420	70	
170503n6	UCL	P2	P10	LG	1×10^{10}	83	1	1935	639	2574	31	1/2 (30 µm)
				TA	5×10^{9}	55		1887	315	2202	40	
170125n3	UCL	P2	P10	LG	5×10^{9}	39	0	670	107	777	20	1/2 (30 µm)
				MG	5×10^{9}	39		819	307	1126	29	
170508n7	UCL	P2	P10	LG	1×10^{10}	110	3	1955	382	2337	21	1/2 (30 µm)
				MG	5×10^{9}	67		1497	429	1926	29	
170125n7	UCL	P2	P10	TA	5×10^{9}	47	0	907	308	1215	26	1/2 (30 µm)
				PL	5×10^{9}	39		1044	195	1239	32	
170125n8	UCL	P2	P10	TA	5×10^{9}	22	2	920	157	1077	49	1/2 (30 µm)
				PL	5×10^{9}	22		741	83	824	37	
1570	UoG	P1	P10	LG	2×10^{8}	11	-	1111	404	1515	138	1/8 (60 µm)
1571	UoG	P1	P10	LG	2×10^{8}	12	-	688	196	884	74	1/8 (60 µm)
1573	UoG	P1	P10	TA	5×10^{8}	10	-	447	68	515	52	1/8 (60 µm)
1574	UoG	P1	P10	TA	5×10^{8}	14	-	297	26	323	23	1/8 (60 µm)
1577	UoG	P2	P10	LG	2×10^{9}	18	2	313	43	356	20	1/8 (60 µm)
				TA	5×10^{9}	26		688	105	793	31	
1578	UoG	P2	P10	LG	2×10^{9}	21	5	292	34	326	16	1/8 (60 µm)

				TA	5×10^{9}	22		790	130	920	42	
1579	UoG	P2	P10	LG	2×10^{9}	30	1	1023	194	1217	41	1/8 (60 µm)
				MG	5×10^{8}	7		169	19	188	27	
1580	UoG	P2	P10	LG	2×10^{9}	14	0	414	48	462	33	1/8 (60 µm)
				MG	5×10^{8}	8		470	87	557	70	
1605	UoG	P1	P10	MG	1×10^{8}	6	-	412	110	522	87	1/8 (60 µm)
1611	UoG	P1	P10	PL	1×10^{8}	2	-	167	24	191	96	1/8 (60 µm)
1613	UoG	P2	P10	PL	1×10^{8}	1	-	164	16	180	180	1/8 (60 µm)
1639	UoG	P2	P10	TA	2×10^{8}	15	-	591	94	685	46	1/8 (60 µm)
1640	UoG	P2	P10	PL	2×10^{8}	20	-	629	122	751	38	1/8 (60 µm)
1644	UoG	P2	P10	LG	1×10^{8}	1	-	142	32	174	174	1/8 (60 µm)
				TA	2×10^{8}	-		57	11	68	-	
1646	UoG	P2	P10	LG	1×10^{8}	1	-	90	16	106	106	1/8 (60 µm)
				TA	2×10^{8}	3		76	13	89	30	
1653	UoG	P2	P10	LG	1×10^{8}	2	-	60	6	66	33	1/8 (60 µm)
				TA	2×10^{8}	2		58	8	66	33	
1656	UoG	P2	P10	LG	1×10^{8}	-	-	563	145	708	-	1/8 (60 µm)
1657	UoG	P2	P10	LG	1×10^{8}	1	-	323	51	374	374	1/8 (60 µm)
1660	UoG	P2	P10	MG	2×10^{8}	7	-	509	3	512	73	1/8 (60 µm)
1661	UoG	P2	P10	MG	2×10^{8}	10	-	175	63	238	24	1/8 (60 µm)
1662	UoG	P2	P10	MG	2×10^{8}	10	-	375	230	605	61	1/8 (60 µm)
1701	UoG	P2	P10	LG	2×10^{9}	8	2	169	26	195	24	1/8 (60 µm)
				MG	5×10^{9}	34		594	190	784	23	
1702	UoG	P2	P10	LG	2×10^{9}	14	2	561	107	668	48	1/8 (60 µm)
				MG	5×10^{9}	2		76	11	87	44	
353	MDC	P4	P10	GS	1×10^{9}	31	-	1542	431	1973	64	All (40 µm)

399	MDC	P4	P10	GS	1×10^9	41	-	569	77	646	16	All (40 µm)
1332	MDC	P4	P10	GS	1×10^9	18	-	1605	323	1928	107	All (40 µm)
1349	MDC	P4	P10	GS	1×10^9	18	-	1416	459	1875	104	All (40 µm)
700	MDC	P4	P10	TA	1×10^9	47	-	1723	122	1845	39	All (40 µm)
721	MDC	P4	P10	TA	1×10^9	22	-	1934	465	2399	109	All (40 µm)
1324	MDC	P4	P10	TA	1×10^9	17	-	2041	301	2342	138	All (40 µm)

731 Table 1: details of individual experiments performed in the three different laboratories (University College London, UCL, University of
732 Glasgow, UoG, Max Delbrück Center for Molecular Medicine, MDC), with individual cell count and virus concentration. Same experimental
733 code as in Figure 2D and Supplementary figures.
734

Method	Pros	Cons	Outcome	Reference
Muscle injection of AAV-G (serotype 2.6) + RabV (Figure 1A)	Avoids the possibility of retrograde disynaptic transfer from second order motor neurons due to restriction of G expression to targeted motor neurons	The labelled premotor population could be contaminated by anterogradely labelled neurons from primary sensory neurons.	Flexor- extensor segregation	(Tripodi et al., 2011)
	Avoids the possibility of retrograde disynaptic transfer from premotor spinal interneurons.	AAV might have unreported specificity for subsets of motor neurons in the pool		
Muscle injection of AAV-flex-G (serotype 2.6) + RabV in *ChAT::Cre* mice (Figure 1B)	Avoids the possibility of retrograde disynaptic transfer from second order motor neurons due to restriction of G expression to targeted motor neurons	AAV might have unreported specificity for subsets of motor neurons in the pool	Flexor- extensor segregation	(Wang et al., 2017)
	Avoids the possibility of retrograde disynaptic transfer from premotor spinal interneurons.			
	Avoids potential anterograde sensory contamination.			
Central injection of AAV-flex-G (serotype 2.9) in *ChAT::Cre* mice followed by muscle injection of RabV, in adults (Figure 1C)	Limits the issue of potential disynaptic transfer from cholinergic interneurons	Potential for disynaptic transfer from cholinergic premotor interneurons, transsynaptically labelled motor neurons and mis-targeted primary motor neurons	Flexor- extensor segregation	(Takeoka and Arber, 2019)
	Avoids potential anterograde tracing from sensory neurons	AAV might have unreported specificity for subsets of motor neurons in the pool		
	Avoids potential anterograde tracing from sensory neurons	Potential for disynaptic transfer from premotor spinal interneurons, transsynaptically labelled	No flexor- extensor segregation	Present study

Genetically driven expression of G in *ChAT::Cre or Olig2::Cre* mice + muscle RabV injection in neonates (Figure 1D and E)	Ensures homogenous expression of G in all motor neurons	motor neurons and mis-targeted primary motor neurons.		
Patch tracing. TVA and G delivery through patch pipette, followed by central administration of the EnvA-RabV (Figure 1F)	Highly specific determination of starter motor neurons. Disambiguates the nature of the premotor network to different types of motor neurons within the same pool.	Single or small pool of starter motor neurons Patching motor neurons in vivo has not yet been proven possible	To be tested	N/A

735 Table 2: Summary of pros and cons of each described method

736

737

738 **References**

739 Bacskai T, Rusznak Z, Paxinos G, Watson C (2013) Musculotopic organization of the motor
740 neurons supplying the mouse hindlimb muscles: a quantitative study using Fluoro-
741 Gold retrograde tracing. Brain Struct Funct Available at:
742 http://www.ncbi.nlm.nih.gov/pubmed/23288256.

743 Bhumbra GS, Beato M (2018) Recurrent excitation between motoneurones propagates
744 across segments and is purely glutamatergic. PLoS Biology 16.

745 Bhumbra GS, Dyball RE (2010) Reading between the spikes of the hypothalamic neural
746 code. J Neuroendocrinol 22:1239–1250.

747 Callaway EM, Luo L (2015) Monosynaptic Circuit Tracing with Glycoprotein-Deleted Rabies
748 Viruses. J Neurosci 35:8979–8985.

749 Castle MJ, Turunen HT, Vandenberghe LH, Wolfe JH (2016) Controlling AAV Tropism in the
750 Nervous System with Natural and Engineered Capsids. In: Gene Therapy for
751 Neurological Disorders: Methods and Protocols (Manfredsson FP, ed), pp 133–149
752 Methods in Molecular Biology. New York, NY: Springer. Available at:
753 https://doi.org/10.1007/978-1-4939-3271-9_10 [Accessed November 24, 2020].

754 Chatterjee S et al. (2018) Nontoxic, double-deletion-mutant rabies viral vectors for
755 retrograde targeting of projection neurons. Nat Neurosci 21:638–646.

756 Chen J-A, Huang Y-P, Mazzoni EO, Tan GC, Zavadil J, Wichterle H (2011) Mir-17-3p
757 Controls Spinal Neural Progenitor Patterning by Regulating Olig2/Irx3 Cross-
758 Repressive Loop. Neuron 69:721–735.

759 Ciabatti E, González-Rueda A, Mariotti L, Morgese F, Tripodi M (2017) Life-Long Genetic
760 and Functional Access to Neural Circuits Using Self-Inactivating Rabies Virus. Cell
761 170:382-392.e14.

762 Dessaud E, Yang LL, Hill K, Cox B, Ulloa F, Ribeiro A, Mynett A, Novitch BG, Briscoe J
763 (2007) Interpretation of the sonic hedgehog morphogen gradient by a temporal
764 adaptation mechanism. Nature 450:717–720.

765 Hultborn H, Jankowska E, Lindstrom S (1971) Recurrent inhibition of interneurones
766 monosynaptically activated from group Ia afferents. The Journal of Physiology Online
767 215:613–636.

768 Jankowska E (2001) Spinal interneuronal systems: identification, multifunctional character
769 and reconfigurations in mammals. J Physiol 533:31–40.

770 Manuel M, Zytnicki D (2019) Molecular and electrophysiological properties of mouse
771 motoneuron and motor unit subtypes. Curr Opin Physiol 8:23–29.

772 Marshel JH, Mori T, Nielsen KJ, Callaway EM (2010) Targeting single neuronal networks for
773 gene expression and cell labeling in vivo. Neuron 67:562–574.

774 McHanwell S, Biscoe TJ (1981) The localization of motoneurons supplying the hindlimb
775 muscles of the mouse. Philos Trans R Soc Lond B Biol Sci 293:477–508.

776 Ohara S, Inoue K, Witter MP, Iijima T (2009a) Untangling neural networks with dual
777 retrograde transsynaptic viral infection. Front Neurosci 3 Available at:
778 https://www.frontiersin.org/articles/10.3389/neuro.01.032.2009/full [Accessed
779 November 18, 2020].

780 Ohara S, Inoue K, Yamada M, Yamawaki T, Koganezawa N, Tsutsui K-I, Witter MP, Iijima T
781 (2009b) Dual transneuronal tracing in the rat entorhinal-hippocampal circuit by
782 intracerebral injection of recombinant rabies virus vectors. Front Neuroanat 3
783 Available at: https://www.frontiersin.org/articles/10.3389/neuro.05.001.2009/full
784 [Accessed November 18, 2020].

785 Osakada F, Callaway EM (2013) Design and generation of recombinant rabies virus vectors.
786 Nature Protocols 8:1583–1601.

787 Rancz EA, Franks KM, Schwarz MK, Pichler B, Schaefer AT, Margrie TW (2011) Transfection
788 via whole-cell recording in vivo: bridging single-cell physiology, genetics and
789 connectomics. Nat Neurosci 14:527–532.

790 Reardon TR, Murray AJ, Turi GF, Wirblich C, Croce KR, Schnell MJ, Jessell TM, Losonczy A
791 (2016) Rabies Virus CVS-N2c Strain Enhances Retrograde Synaptic Transfer and
792 Neuronal Viability. Neuron Available at:
793 http://www.ncbi.nlm.nih.gov/pubmed/26804990.

794 Romanes GJ (1964) THE MOTOR POOLS OF THE SPINAL CORD. Prog Brain Res 11:93–
795 119.

796 Rossi J, Balthasar N, Olson D, Scott M, Berglund E, Lee CE, Choi MJ, Lauzon D, Lowell BB,
797 Elmquist JK (2011) Melanocortin-4 Receptors Expressed by Cholinergic Neurons
798 Regulate Energy Balance and Glucose Homeostasis. Cell Metabolism 13:195–204.

799 Skarlatou S, Hérent C, Toscano E, Mendes CS, Bouvier J, Zampieri N (2020) Afadin
800 Signaling at the Spinal Neuroepithelium Regulates Central Canal Formation and Gait
801 Selection. Cell Rep 31:107741.

802 Stanek E IV, Cheng S, Takatoh J, Han B-X, Wang F (2014) Monosynaptic premotor circuit
803 tracing reveals neural substrates for oro-motor coordination Mason P, ed. eLife
804 3:e02511.

805 Stepien AE, Tripodi M, Arber S (2010) Monosynaptic rabies virus reveals premotor network
806 organization and synaptic specificity of cholinergic partition cells. Neuron 68:456–
807 472.

808 Sürmeli G, Akay T, Ippolito GC, Tucker PW, Jessell TM (2011) Patterns of Spinal Sensory-
809 Motor Connectivity Prescribed by a Dorsoventral Positional Template. Cell 147:653–
810 665.

811 Takatoh J, Nelson A, Zhou X, Bolton MM, Ehlers MD, Arenkiel BR, Mooney R, Wang F
812 (2013) New modules are added to vibrissal premotor circuitry with the emergence of
813 exploratory whisking. Neuron 77:346–360.

814 Takeoka A, Arber S (2019) Functional Local Proprioceptive Feedback Circuits Initiate and
815 Maintain Locomotor Recovery after Spinal Cord Injury. Cell Reports 27:71-85.e3.

816 Todd AJ, Sullivan AC (1990) Light microscope study of the coexistence of GABA-like and
817 glycine-like immunoreactivities in the spinal cord of the rat. Journal of Comparative
818 Neurology 296:496–505.

819 Todd AJ, Watt C, Spike RC, Sieghart W (1996) Colocalization of GABA, glycine, and their
820 receptors at synapses in the rat spinal cord. J Neurosci 16:974–982.

821 Towne C, Schneider BL, Kieran D, Redmond DE, Aebischer P (2010) Efficient transduction
822 of non-human primate motor neurons after intramuscular delivery of recombinant
823 AAV serotype 6. Gene Therapy 17:141–146.

824 Tripodi M, Stepien AE, Arber S (2011) Motor antagonism exposed by spatial segregation and
825 timing of neurogenesis. Nature 479:61–66.

826 Ugolini G (2011) Rabies Virus as a Transneuronal Tracer of Neuronal Connections.

827 Wall NR, Wickersham IR, Cetin A, De La Parra M, Callaway EM (2010) Monosynaptic circuit
828 tracing in vivo through Cre-dependent targeting and complementation of modified
829 rabies virus. Proc Natl Acad Sci U S A 107:21848–21853.

830 Wang X, Liu Y, Li X, Zhang Z, Yang H, Zhang Y, Williams PR, Alwahab NSA, Kapur K, Yu B,
831 Zhang Y, Chen M, Ding H, Gerfen CR, Wang KH, He Z (2017) Deconstruction of
832 Corticospinal Circuits for Goal-Directed Motor Skills. Cell 171:440-455.e14.

833 Wickersham IR, Lyon DC, Barnard RJ, Mori T, Finke S, Conzelmann KK, Young JA,
834 Callaway EM (2007) Monosynaptic restriction of transsynaptic tracing from single,
835 genetically targeted neurons. Neuron 53:639–647.

836 Zagoraiou L, Akay T, Martin JF, Brownstone RM, Jessell TM, Miles GB (2009) A Cluster of
837 Cholinergic Premotor Interneurons Modulates Mouse Locomotor Activity. Neuron
838 64:645–662.

839 Zampieri N, Jessell TM, Murray AJ (2014) Mapping sensory circuits by anterograde
840 transsynaptic transfer of recombinant rabies virus. Neuron 81:766–778.

841 Zeilhofer HU, Studler B, Arabadzisz D, Schweizer C, Ahmadi S, Layh B, Bosl MR, Fritschy
842 JM (2005) Glycinergic neurons expressing enhanced green fluorescent protein in
843 bacterial artificial chromosome transgenic mice. J Comp Neurol 482:123–141.

844

Figure 1

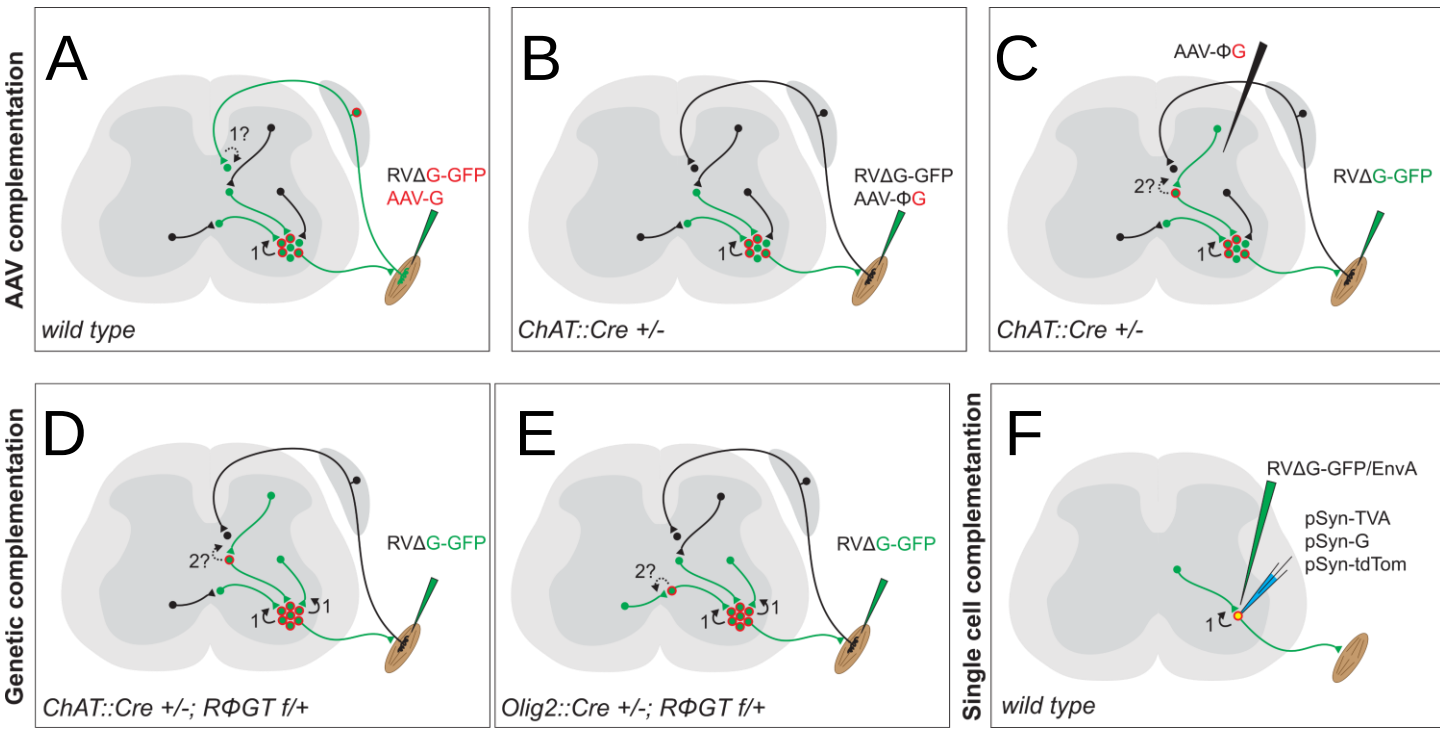
AAV complementation
A
1?
RVΔG-GFP
AAV-G
1
wild type
B
RVΔG-GFP
AAV-ΦG
1
ChAT::Cre +/-
C
AAV-ΦG
2?
RVΔG-GFP
1
ChAT::Cre +/-
Genetic complementation
D
2?
RVΔG-GFP
1
1
ChAT::Cre +/-; RΦGT f/+
E
2?
RVΔG-GFP
1
1
Olig2::Cre +/-; RΦGT f/+
Single cell complemetantion
F
RVΔG-GFP/EnvA
pSyn-TVA
pSyn-G
pSyn-tdTom
1
wild type

Figure 2

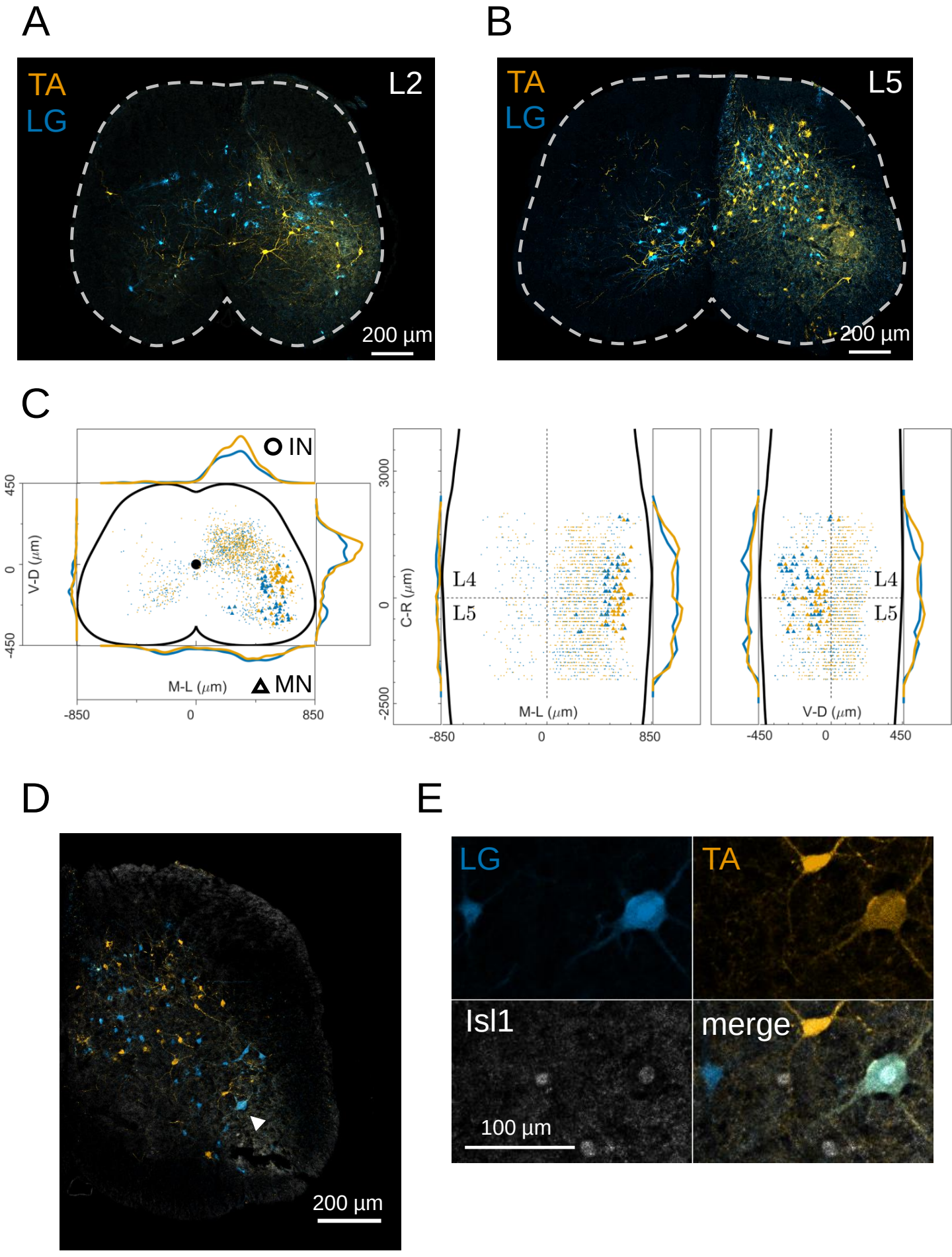
A
TA
LG
L2
200 µm
B
TA
LG
L5
200 µm
C
IN
MN
V-D (µm)
M-L (µm)
C-R (µm)
L4
L5
D
200 µm
E
LG
TA
Isl1
merge
100 µm

Figure 3

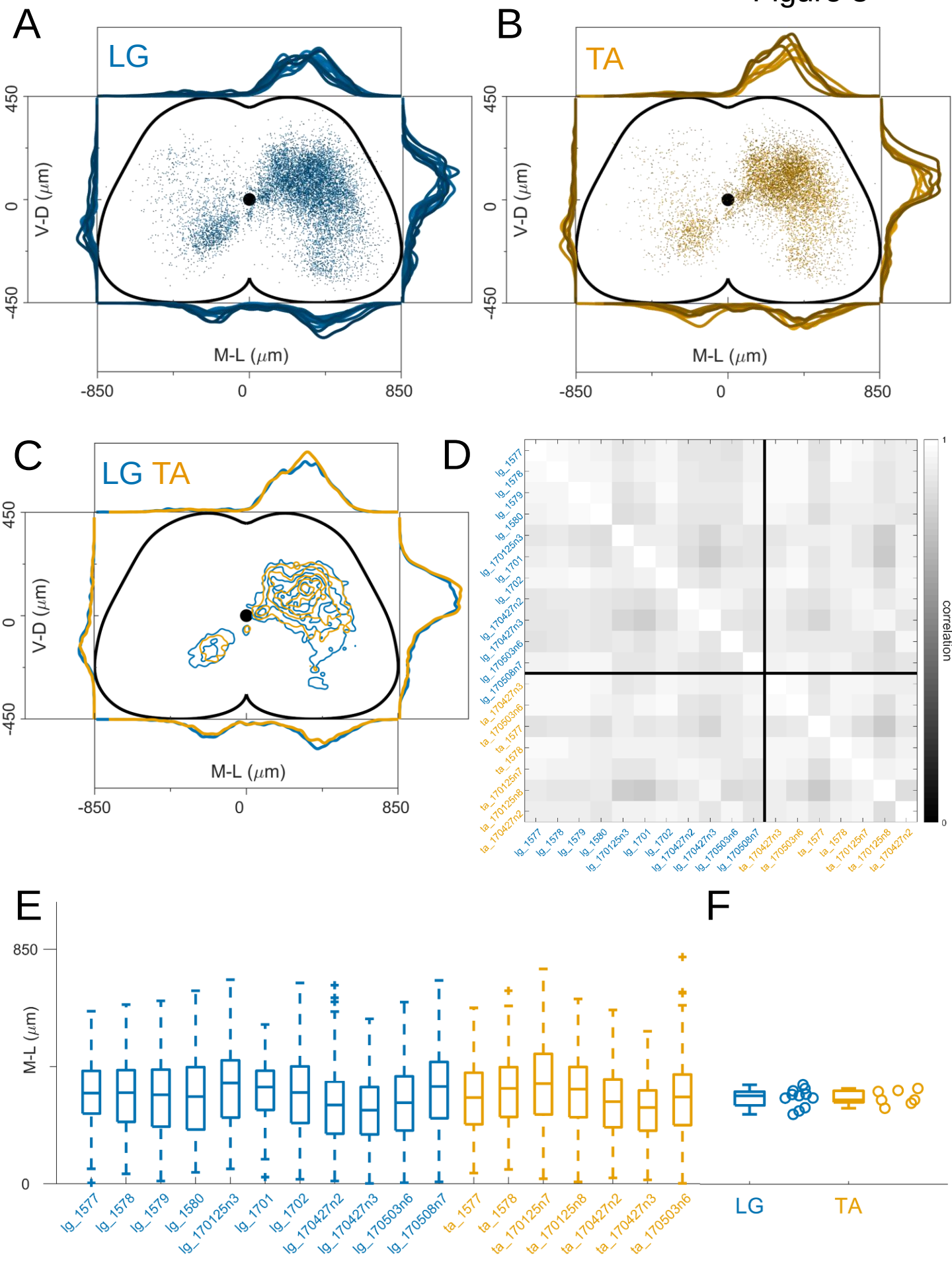
A
LG
B
TA
C
LG TA
D
E
F
V-D (μm)
M-L (μm)
450
0
-450
-850
850
correlation
1
lg_1577
lg_1578
lg_1579
lg_1580
lg_170125n3
lg_1701
lg_1702
lg_170427n2
lg_170427n3
lg_170503n6
lg_170508n7
ta_170427n3
ta_170503n6
ta_1577
ta_1578
ta_170125n7
ta_170125n8
ta_170427n2
LG
TA

Figure 4

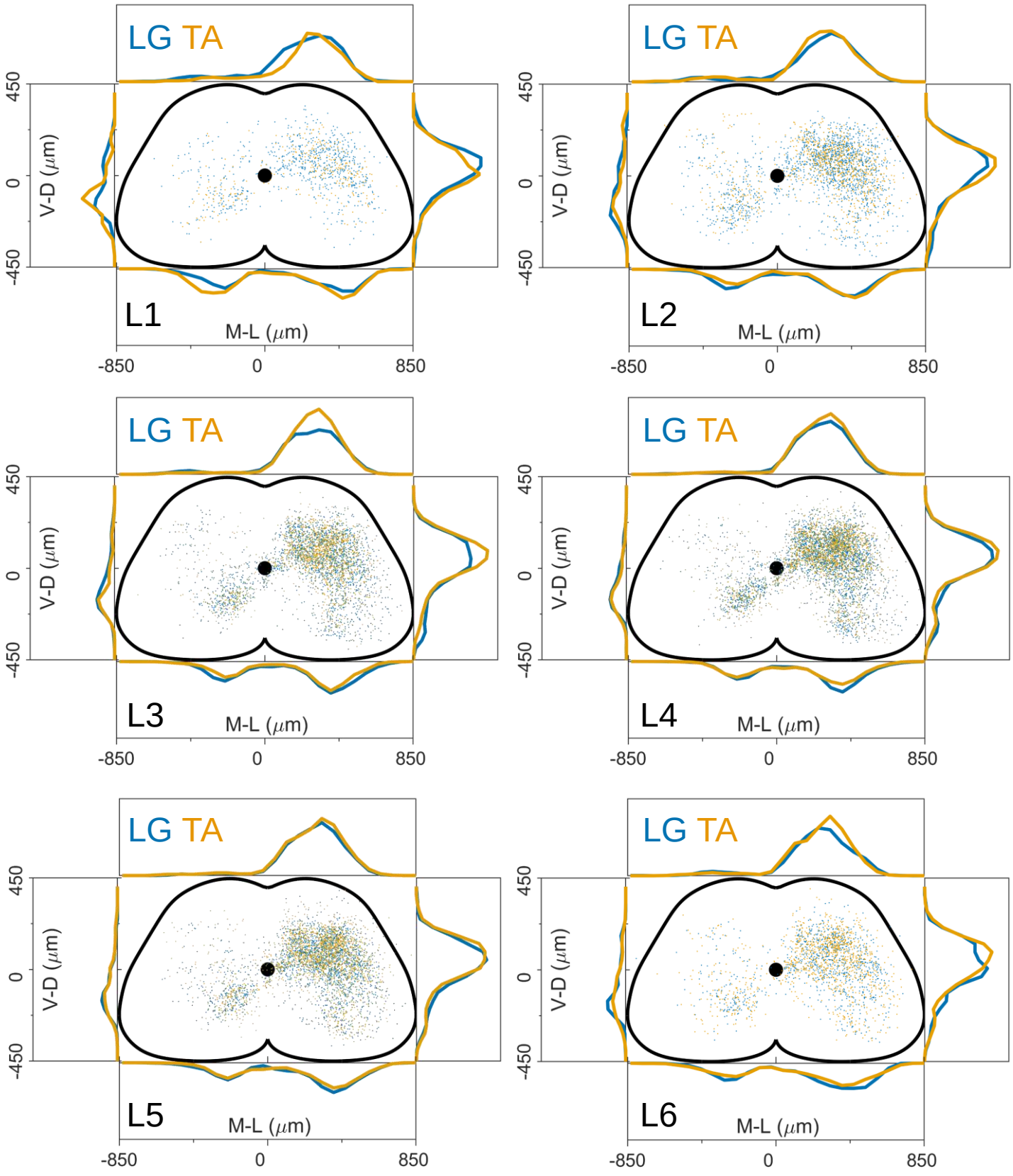

Figure 5

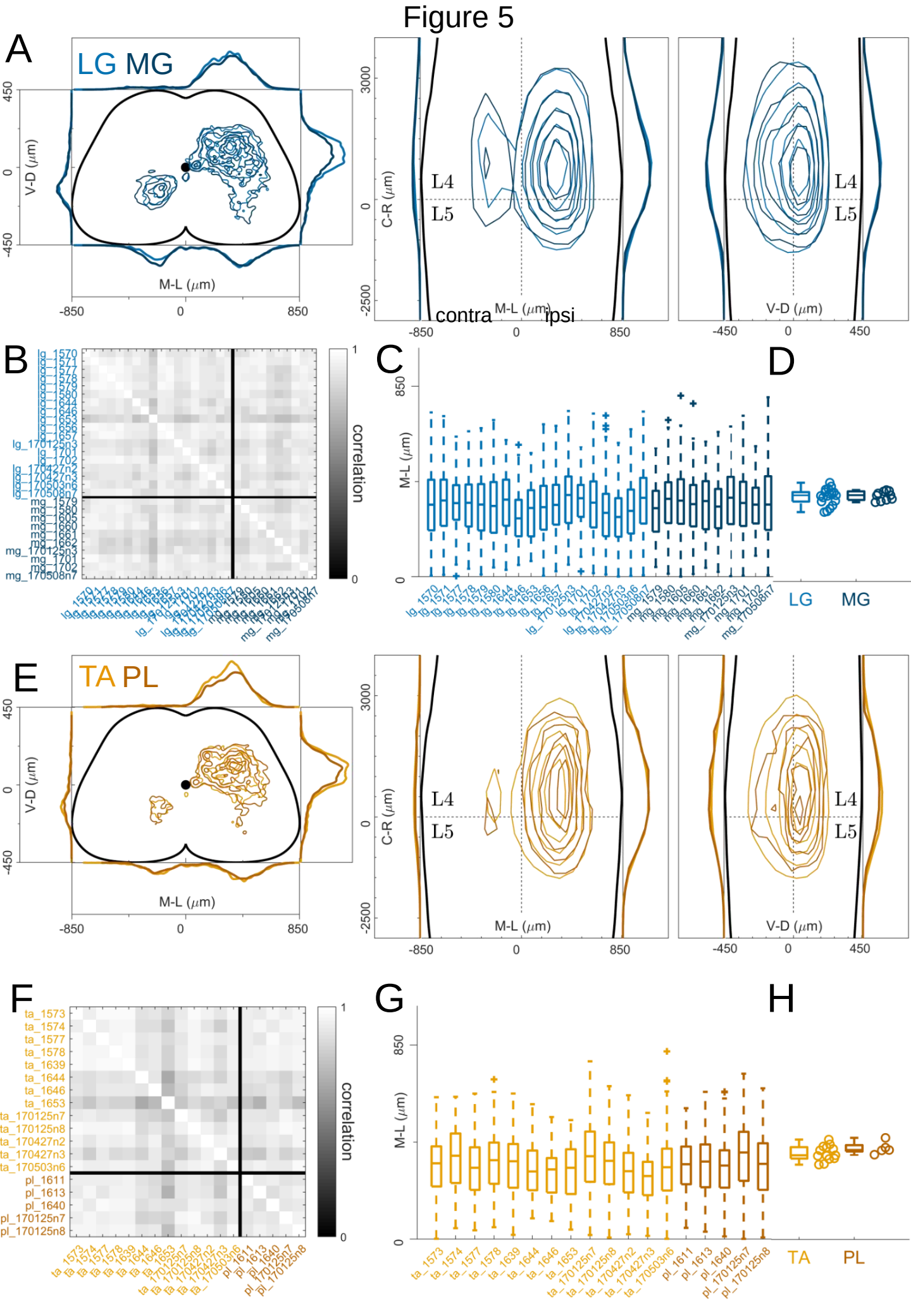
A
LG MG
V-D (μm)
M-L (μm)
C-R (μm)
L4
L5
contra
ipsi
B
correlation
C
D
LG
MG
E
TA PL
F
G
H
TA
PL

Figure 6

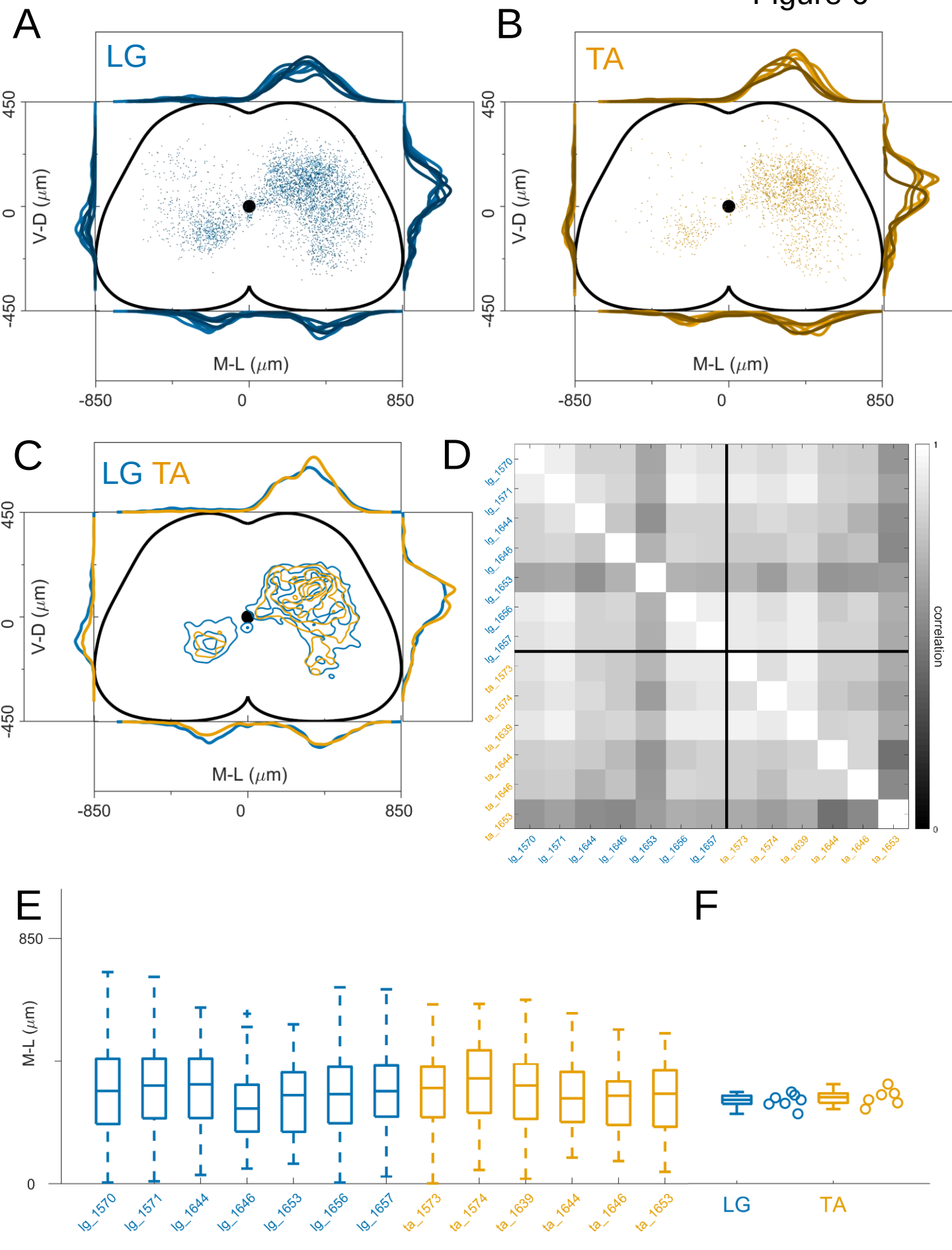
A
LG
B
TA
C
LG TA
D
E
F
V-D (μm)
M-L (μm)
450
0
-450
-850
850
correlation
1
lg_1570
lg_1571
lg_1644
lg_1646
lg_1653
lg_1656
lg_1657
ta_1573
ta_1574
ta_1639
ta_1644
ta_1646
ta_1653
LG
TA

Figure 7

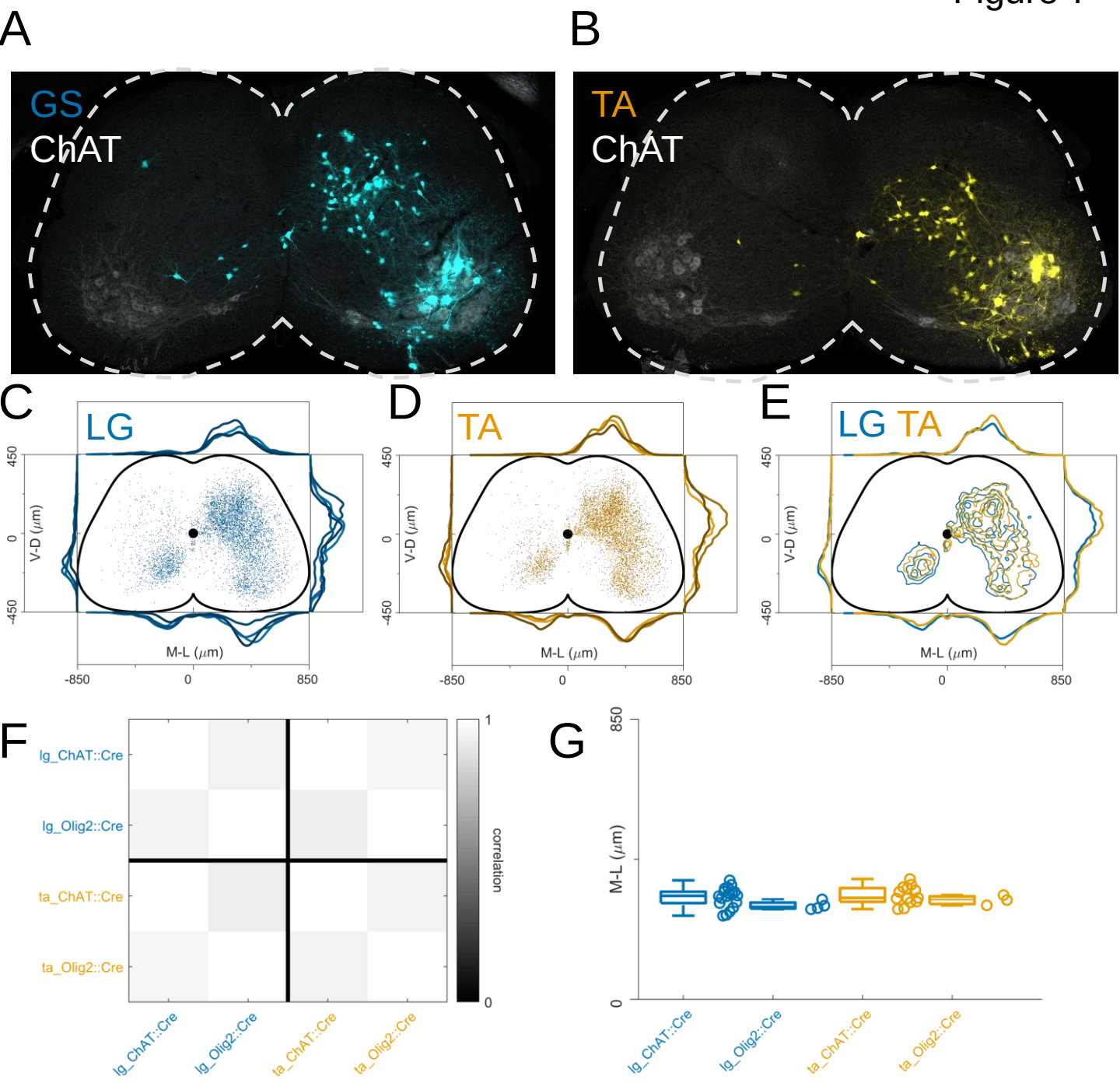
A
GS
ChAT
B
TA
ChAT
C
LG
D
TA
E
LG TA
V-D (μm)
M-L (μm)
450
0
-450
-850
850
F
lg_ChAT::Cre
lg_Olig2::Cre
ta_ChAT::Cre
ta_Olig2::Cre
correlation
1
0
G
M-L (μm)
850
0

Figure 8

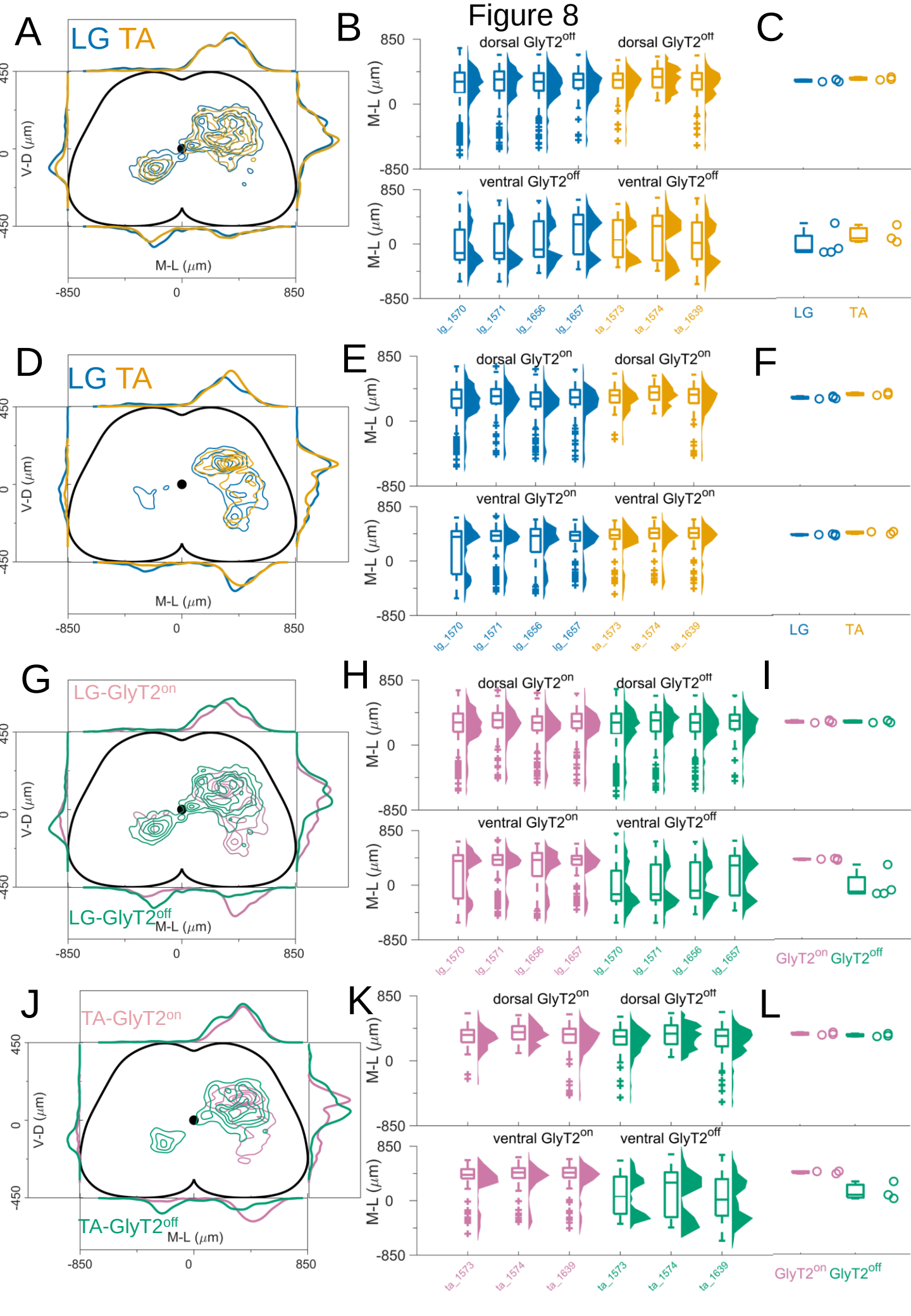
A
LG TA
V-D (μm)
M-L (μm)
B
dorsal GlyT2off
dorsal GlyT2off
ventral GlyT2off
ventral GlyT2off
M-L (μm)
lg_1570
lg_1571
lg_1656
lg_1657
ta_1573
ta_1574
ta_1639
C
LG
TA
D
LG TA
E
dorsal GlyT2on
dorsal GlyT2on
ventral GlyT2on
ventral GlyT2on
F
G
LG-GlyT2on
LG-GlyT2off
H
dorsal GlyT2on
dorsal GlyT2off
ventral GlyT2on
ventral GlyT2off
I
GlyT2on GlyT2off
J
TA-GlyT2on
TA-GlyT2off
K
dorsal GlyT2on
dorsal GlyT2off
ventral GlyT2on
ventral GlyT2off
L
GlyT2on GlyT2off